Cell Reports
Medicine

Article

Gestational palmitic acid suppresses embryonic GATA-binding protein 4 signaling and causes congenital heart disease

Graphical abstract

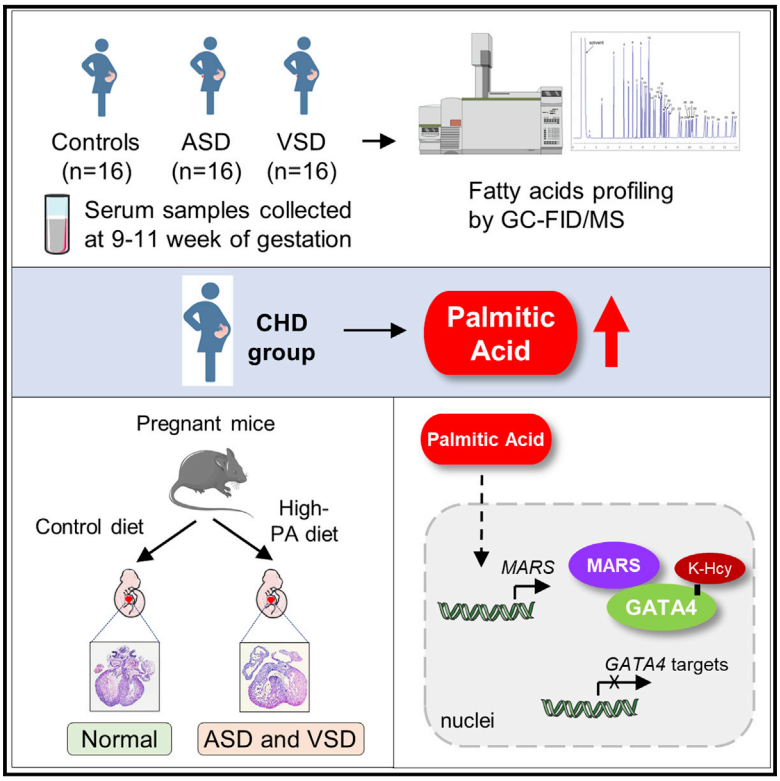

Highlights

- Maternal high palmitic acid is associated with increased risk of CHD in offspring
- Palmitic acid promotes MARS and K-Hcy modification through activating NF-κB
- GATA4 transcriptional acitivity is inhibited by K-Hcy modification
- Inhibition of K-Hcy rescued PA-induced CHD occurrence in mice

Authors

Rui Zhao, Li Cao, Wen-Jun Gu, ..., Jing Cao, Kun Sun, Jian-Yuan Zhao

Correspondence

husq04@163.com (X.-Y.Z.), caojing73@126.com (J.C.), sunkun@xinhuamed.com.cn (K.S.), zhaojy@vip.163.com (J.-Y.Z.)

In brief

Zhao et al. report that elevated maternal serum palmitic acid (PA) is associated with the risk of congenital heart disease (CHD) in offspring. PA induces CHD phenotypes in mice via promoting K-Hcy of GATA4, therefore inhibiting its transcriptional activity. Inhibition of K-Hcy rescued PA-induced CHD occurrence.

Zhao et al., 2023, Cell Reports Medicine *4*, 100953
March 21, 2023
https://doi.org/10.1016/j.xcrm.2023.100953

CellPress

Cell Reports Medicine

CellPress
OPEN ACCESS

Article

Gestational palmitic acid suppresses embryonic GATA-binding protein 4 signaling and causes congenital heart disease

Rui Zhao,[1,7] Li Cao,[2,7] Wen-Jun Gu,[2,7] Lei Li,[3,7] Zhong-Zhong Chen,[4,7] Jie Xiang,[2] Ze-Yu Zhou,[2] Bo Xu,[5] Wei-Dong Zang,[3] Xiang-Yu Zhou,[2,*] Jing Cao,[3,*] Kun Sun,[1,*] and Jian-Yuan Zhao[1,3,6,8,*]

[1]Institute for Developmental and Regenerative Cardiovascular Medicine, MOE-Shanghai Key Laboratory of Children's Environmental Health, Xinhua Hospital, Shanghai Jiao Tong University School of Medicine, Shanghai 200092, China

[2]Obstetrics & Gynecology Hospital of Fudan University, State Key Lab of Genetic Engineering, School of Life Sciences, and Department of Materials Science, Fudan University, Shanghai 200438, China

[3]Department of Anatomy and Neuroscience Research Institute, School of Basic Medical Sciences, Zhengzhou University, Zhengzhou 450001, China

[4]Urogenital Development Research Center, Department of Urology, Shanghai Children's Hospital School of Medicine, Shanghai Jiao Tong University, Shanghai 200062, China

[5]Department of Anesthesiology, General Hospital of Southern Theatre Command of People's Liberation Army, Guangzhou 510030, China

[6]International Human Phenome Institutes (Shanghai), Shanghai 200433, China

[7]These authors contributed equally

[8]Lead contact

*Correspondence: husq04@163.com (X.-Y.Z.), caojing73@126.com (J.C.), sunkun@xinhuamed.com.cn (K.S.), zhaojy@vip.163.com (J.-Y.Z.)

https://doi.org/10.1016/j.xcrm.2023.100953

SUMMARY

Dysregulated maternal fatty acid metabolism increases the risk of congenital heart disease (CHD) in offspring with an unknown mechanism, and the effect of folic acid fortification in preventing CHD is controversial. Using gas chromatography coupled to either a flame ionization detector or mass spectrometer (GC-FID/MS) analysis, we find that the palmitic acid (PA) concentration increases significantly in serum samples of pregnant women bearing children with CHD. Feeding pregnant mice with PA increased CHD risk in offspring and cannot be rescued by folic acid supplementation. We further find that PA promotes methionyl-tRNA synthetase (MARS) expression and protein lysine homocysteinylation (K-Hcy) of GATA4 and results in GATA4 inhibition and abnormal heart development. Targeting K-Hcy modification by either genetic ablation of *Mars* or using *N*-acetyl-L-cysteine (NAC) decreases CHD onset in high-PA-diet-fed mice. In summary, our work links maternal malnutrition and MARS/K-Hcy with the onset of CHD and provides a potential strategy in preventing CHD by targeting K-Hcy other than folic acid supplementation.

INTRODUCTION

Congenital heart disease (CHD), the most common congenital human birth defect, affects 9.1 per 1,000 live births worldwide.[1] CHD onset is influenced by both genetic and nutritional factors.[2] The periconceptional administration of folic acid, which is a synthetic form of folate, is the most effective method for CHD prevention. Epidemiological studies have shown that folic acid fortification reduces the risk of CHD in newborns,[3–5] whereas exposure to folic acid antagonists during pregnancy increases the risk of CHD in offspring.[6]

Our previous genetic and biochemical studies revealed that folic acid supplementation may mainly reduce homocysteine levels in cells, the elevation of which causes CHD. Genetic noncoding variations in homocysteine removal genes, including methionine synthase (*MTR*), *MTR* reductase (*MTRR*), and cystathionine β-synthase (*CBS*), decrease the expression of these genes and lead to the accumulation of homocysteine, thereby increasing the risk of CHD.[7–9] Moreover, increased proteasome activity-mediated folate transmembrane transport decreases the risk of CHD by reducing homocysteine levels.[10] With regards to the mechanisms underlying the teratogenic effects of homocysteine, we found that increased homocysteine levels could be sensed by methionyl-tRNA synthetase (MARS), leading to the lysine homocysteinylation (K-Hcy) modification of proteins and generation of K-Hcy signals.[11] Increased K-Hcy levels inhibit developmental signals and lead to birth defects. In human genetic studies, we observed increased copy numbers of *MARS* and/or *MARS2* in patients with CHD, validating the pathological effects of K-Hcy.[12] These findings suggest that teratogenic K-Hcy levels are determined by both the substrate homocysteine and enzyme MARS.[13] Although K-Hcy could be alleviated by lowering homocysteine levels using folic acid supplementation, which is performed globally, the incidence of CHD has increased significantly in recent years due to unknown reasons.[1,9]

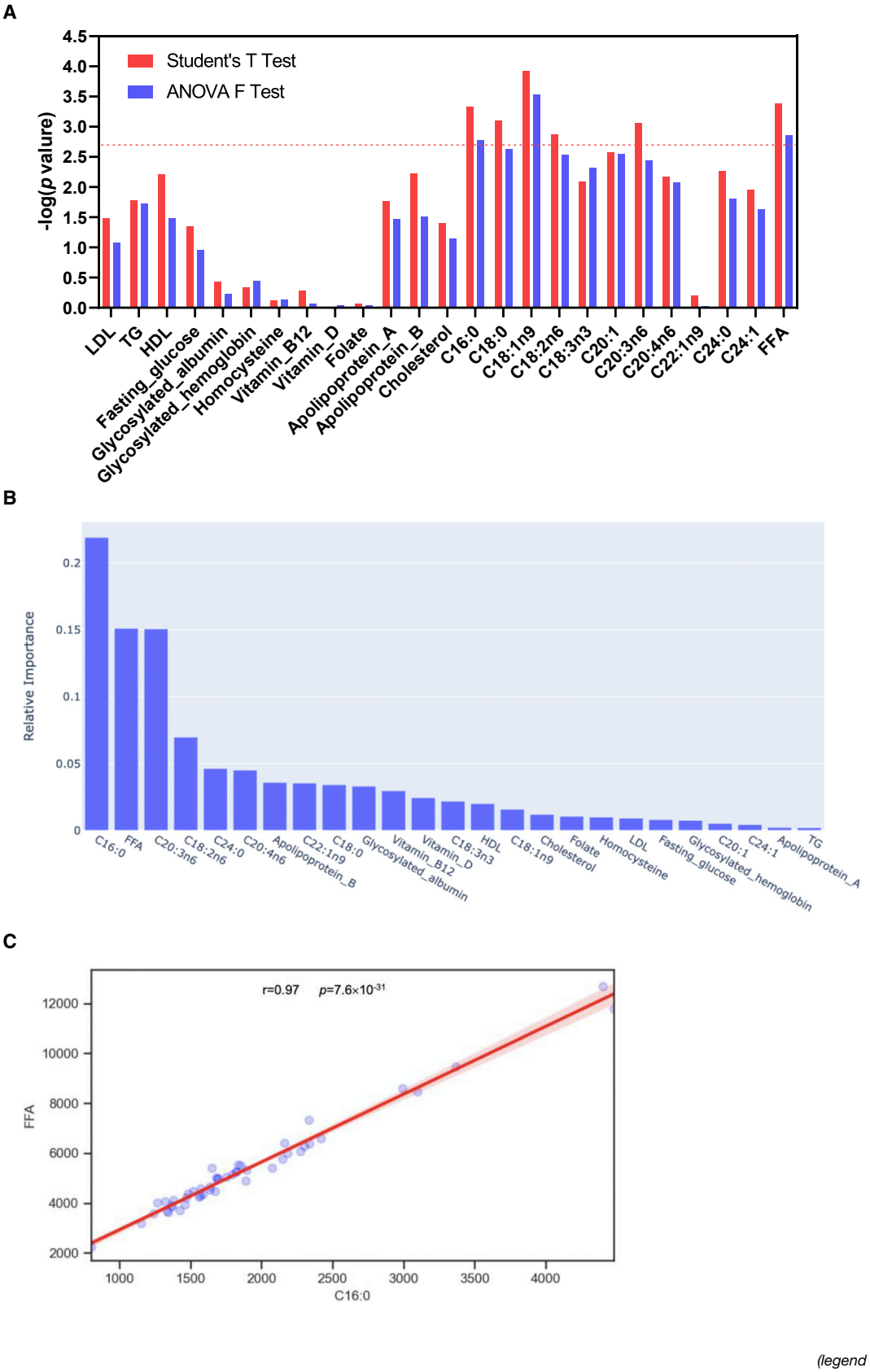

(legend on next page)

In addition to folate-homocysteine balance, dysregulated maternal lipid metabolism contributes to the risk of CHD in offspring. For example, maternal obesity is associated with numerous pregnancy-related adverse outcomes, including an increased risk of congenital septal anomalies and neural tube defects.[2,4,14–17] In addition, high maternal triglyceride (TG) levels during early pregnancy are associated with an increased risk of CHD in offspring.[18] A high-fat diet during pregnancy also increases this risk, as shown by human cohort[19] and animal model studies.[20,21] Considering that fatty acids play a central role in embryonic development,[22,23] these findings suggest that increased maternal circulating fatty acids may increase the risk of CHD in offspring by changing the developmental environment of the embryo. However, the mechanisms by which increased fatty acids generate teratogenic signals are unknown.

We previously found that a high-fat diet activates MARS expression in several organs of mice, suggesting a potential relationship between fatty acids and K-Hcy signals.[24] Considering that a high-fat diet is correlated with dysregulated MARS and K-Hcy levels and that free fatty acids (FFAs) have a signaling role in cells, we hypothesized that imbalanced maternal fatty acids may affect embryonic MARS expression, amplify the signal from homocysteine independent of folate or folic acid effects, and increase the risk of CHD in offspring. In this study, we aimed to identify CHD-related FFAs in serum samples obtained from pregnant women. In addition, we used *in vitro* assays, cell cultures, and mouse models to investigate how imbalanced FFA levels increase the risk of CHD by attenuating the CHD-protective effect of folate.

RESULTS

Increased serum palmitic acid levels during early pregnancy are associated with increased CHD risk in offspring

To investigate whether FFAs were associated with the risk of CHD, we screened FFA levels in the serum samples of 32 pregnant women bearing children with CHD and 16 pregnant women bearing healthy children (Figure S1A). The screening was performed using gas chromatography coupled to either a flame ionization detector or mass spectrometer (GC-FID/MS). In total, 11 types of FFAs and total FFA levels were successfully determined (Table S1; Figure S1B). In addition, the levels of 13 nutrients were measured using conventional clinical methods, including established CHD-related maternal nutrition factors, such as TGs, folate, vitamin B12, and homocysteine (Table S2). We compared the serum concentrations of maternal metabolites between pregnant women bearing children with CHD and those bearing healthy children and found that the levels of FFA types and total FFA increased significantly in pregnant women bearing children with CHD (Table S1; Figures S1C–S1M).

Two statistical models, including the two-tailed t test and ANOVA *F* test, were used to analyze 25 types of serum nutrients, including 11 types of FFAs, total FFA levels, and 13 nutrients measured using conventional clinical methods, to identify significant features (Figure 1A). The association was assumed to be significant after Bonferroni correction at $p < 2.0 \times 10^{-3}$ (0.05/25). C16:0, C18:0, C18:1n9, C18:2n6, C20:3n6, and FFAs were significant after t tests with Bonferroni corrections. All FFAs showed strong correlations with each other (Pearson's correlation coefficient > 0.8; Figure S1N). After combining the *F* tests and performing Bonferroni corrections, maternal palmitic acid (PA; C16:0), oleic acid (C18:1n9), and total FFA levels were significant. A permutation test performed by randomly shuffling the values based on the random forest model indicated that PA, total FFA, and eicosatrienoic acid (C20:3n6) were the top three important fatty acid types (Figure 1B). Maternal PA and total FFA showed a strong correlation (Pearson's correlation coefficient = 0.99, $p = 1.2 \times 10^{-40}$; Figure 1C) and were the two most promising fatty acid types associated with CHD risk.

Elevated PA levels in pregnant mice induce the onset of CHD

We explored whether increased levels of maternal PA indeed caused, and were not just correlated with, CHD in offspring. We assessed the teratogenic effects of PA in a mouse model fed with a high-PA diet. Eight-week-old C57BL/6J female mice were fed high-PA chow prepared by supplementing standard chow diet (CD) with either 0.5% or 1% PA. The ratio of PA to normal chow was optimized to ensure that increased circulating PA levels were comparable to those observed in clinical patients. CD supplemented with 1% PA (10 g/kg added to the standard CD) induced a 50% increase in PA concentration in mouse serum, a rise that mimicked the PA levels observed in clinical patients with CHD compared with the control group (Figure S2A). We also established mouse models with high levels of other fatty acids, which were also increased in the pregnant women bearing children with CHD. These included oleic acid (C18:1n9; Figure S2B), linoleic acid (C18:2n6; Figure S2C), stearic acid (C18:0; Figure S2D), and eicosatrienoic acid (C20:3n6; Figure S2E). Pregnant mice were administered high-fatty-acid chow or normal chow from embryonic day 0.5 (E0.5) to E13.5. Next, the cardiac phenotypes of the embryos at E14.5 were examined using histological analyses. During the feeding period, the high-PA chow did not affect the food intake, water intake, body weight, blood pressure, pulse, blood glucose, glucose tolerance, and fat mass of pregnant mice (Figures S2F–S2N). Moreover, no differences were observed in the total number of fetuses and incidence of absorbed fetuses between the different groups of pregnant mice (Figures S2O and S2P). However, ventricular septal defect (VSD) and atrial septal defect (ASD) phenotypes were observed in the hearts of embryos obtained from high-PA-diet-fed female mice (Figure 2A). The proportion of

Figure 1. Increased serum PA levels during early pregnancy are associated with increased CHD risk in offspring

(A) FFA evidence of association analysis for CHD in offspring using t tests and ANOVA *F* tests. The x axis shows the different FFA levels, and the y axis represents the $-\log_{10}$ p values using the two different models. The dashed horizontal red line indicates the 5% Bonferroni threshold.

(B) Permutation importance showed PA (C16:0) as the most important variable in the random forest model.

(C) Pearson's correlation coefficient was used to correlate the total FFA (y) and C16:0 (x). The Pearson's correlation coefficient was r = 0.97.

A

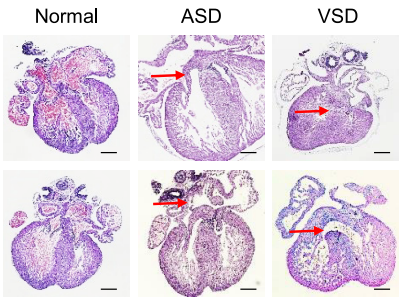

B

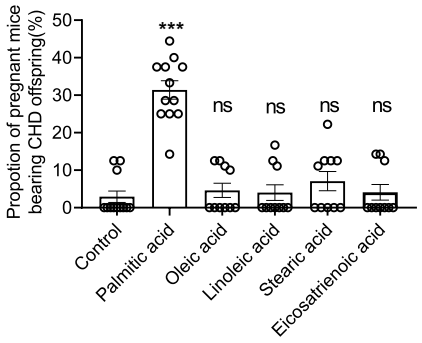

C

Incidence of CHD embryos

	Pregnant mice	Total fetuses	Absorbed fetuses	VSD	ASD	Ratio of CHD	*P* value	RR (95%CI)
Control	12	105	4	2	1	2.97%	/	/
Palmitic Acid	12	103	6	17	14	31.96%	6.4×10^{-8} (***)	10.76 (3.40-34.04)
Oleic Acid	10	83	1	2	2	4.88%	0.78 (ns)	1.64 (0.38-7.13)
Linoleic Acid	10	79	2	2	1	4.00%	0.94 (ns)	1.31 (0.27-6.32)
Stearic Acid	10	81	3	4	2	7.69%	0.28 (ns)	2.59 (0.67-10.03)
Eicosatrienoic Acid	10	79	3	1	2	3.57%	0.95 (ns)	1.33 (0.28-6.40)

D

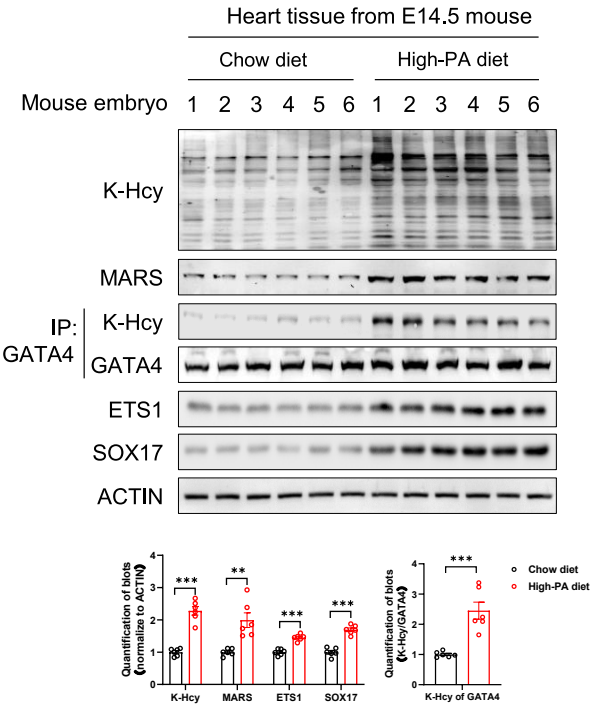

E

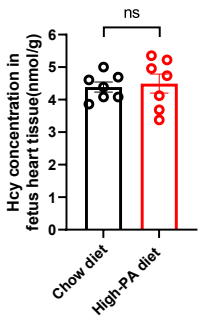

F

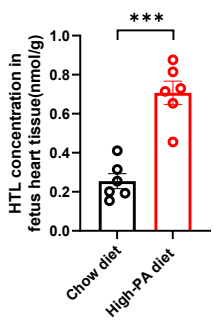

Figure 2. Elevated PA levels in pregnant mice induced CHD onset

(A) CHD phenotypes in embryos from mice with high levels of PA. Representative histological staining results are shown (scale bar, 500 μm).

(B) Proportion of pregnant mice bearing CHD offspring after being fed normal chow and fatty-acid-rich chow (n = 12 mice in the normal and PA groups; n = 10 mice in other groups).

(legend continued on next page)

pregnant mice with offspring having CHD increased from 25% (3 out of 12) in the control group to 100% (12 out of 12) in the high-PA-feeding group (Figure 2B). The CHD occurrence ratio for all offspring significantly increased from 2.97% in the control group (3 in 101) to 31.96% (31 in 97) in the high-PA-diet-fed group, indicating a statistically significant difference between these groups ($p = 6.4 \times 10^{-8}$, relative risk [RR] = 10.78, 95% confidence interval [CI] = 3.40–34.04; Figure 2C). We also evaluated the gender of the embryos and found no differences in the embryos with CHD (Figure S2Q). In contrast, in the mice administered other kinds of high-fatty-acid chow, such as oleic acid, stearic acid, eicosatrienoic acid, or linoleic acid, the incidence of CHD in the offspring did not increase (Figures 2B and 2C). These results suggest that increased maternal PA levels affect heart development and increase the risk of CHD in mouse embryos.

PA levels are associated with increased MARS expression and protein K-Hcy

We explored how increased maternal PA levels led to the occurrence of CHD in offspring. High-fat diets are known to increase the risk of CHD in offspring.[21,25] The findings of our previous study showed that a high-fat diet activated MARS expression and amplified the signal from homocysteine to cause protein K-Hcy modification.[24] Therefore, we hypothesized that PA alone was sufficient to activate MARS, as PA is the predominant form of fatty acids in the high-fat diet (https://researchdiets.com/). By comparing homocysteine, MARS, and K-Hcy levels in mouse heart tissues between embryos from maternal high-PA-diet-fed mice and maternal normal CD-fed mice, we found that MARS expression and K-Hcy levels (Figure 2D), but not homocysteine levels (Figure 2E), were notably increased in the heart tissues of embryos from maternal high-PA-diet-fed mice. As the active form of Hcy in generating K-Hcy modification catalyzed by MARS, homocysteine thiolactone (HTL) levels were significantly increased in embryonic hearts of maternal high-PA-diet-fed mice (Figure 2F). Collected results suggested that PA may activate MARS to generate HTL and promote pan-K-Hcy modification.

Thereafter, we confirmed whether PA activated MARS expression by conducting experiments using cultured cells. We found that, in the cultured mouse cardiac muscle cell line HL-1, rat myoblast cell line H9C2, human embryonic kidney-derived HEK293T cells, and primary neonatal rat ventricular myocytes (NRVMs), elevated PA levels strongly activated both the mRNA (Figure 3A) and protein expression (Figure 3B) of MARS. However, other common FFAs did not cause a significant increase in MARS expression (Figures 3A and 3B). Moreover, elevated PA levels led to dose- and time-dependent increases in MARS expression and pan-K-Hcy levels in HL-1, H9C2, HEK293T, and NRVM cells (Figures 3C and 3D). Folic acid supplementation in the culture media did not reduce pan-K-Hcy levels in PA-treated cells (Figure 3E). Instead, supplementation with *N*-acetyl-L-cysteine (NAC), a well-known antioxidant that also decreased HTL formation (Figure S3A), and MARS enzymatic inhibitor acetyl Hcy thioether (AHT)[12] decreased pan-K-Hcy levels and blocked the effects of PA in promoting K-Hcy (Figures 3E and 3F). These results indicated that PA increased K-Hcy levels by activating MARS expression. To examine whether PA abrogated folate effects by regulating folate metabolism, we measured expression of key folate metabolism enzymes by qRT-PCR in both mice models and HL-1 cells, and it was found that neither *Rfc1*, *Dhfr*, *Mtr*, or *Mthfr* was changed after PA treatment, which conclude the possibility that PA regulates folate metabolism (Figures S3B and S3C). In addition, supplementation with cycloheximide, an RNA synthesis inhibitor, blocked the effects of PA on increasing the MARS protein levels (Figure 3G). Considering that the changing *MARS* mRNA patterns were in accordance with its protein levels (see Figures 3A and 3B), these results indicate that PA increases the transcription levels of *MARS*.

PA increases MARS transcription by activating the NF-κB pathway

To explore how PA activates *MARS* transcription, we predicted potential transcriptional factors in the *MARS* promoter regions in humans, mice, and rats using the online Jaspar database (http://jaspar.genereg.net). We found that RELA, MXI1, MEIS2, TCF4, KLF2, and CEBPA have potential binding sites in the promoter region of *MARS* (Figure S6). The knockdown of RELA, but not of the other transcription factors, led to decreased mRNA levels of *MARS* in cultured HL-1 and HEK293T cells (Figure S5). Considering that RELA, also known as the nuclear factor κB (NF-κB) p65 subunit, was reported to be activated by PA through Toll-like receptor 4,[26] these observations suggest that PA activates *MARS* expression through RELA. Upon NF-κB activation, phosphorylated RELA translocated to the nucleus and bound to the consensus sequence 5′-GGRNNYYCC-3′ (R = A or G, Y = T or C) located in the promoters or enhancers of the target genes. We first confirmed that PA activated the NF-κB pathway in cultured HEK293T and HL-1 cells (Figure 4A). The knockdown of RELA decreased both the mRNA and protein levels of *MARS* and blocked the effect of PA in activating *MARS* expression (Figures 4B and 4C). By conducting *in vitro* electrophoretic mobility shift assays (EMSAs; Figure 4D) and luciferase assays (Figure 4E), we confirmed that RELA binds to the promoter region of *MARS*. Moreover, we validated that RELA bound to the *MARS* promoters in human and mouse cell lines using chromatin immunoprecipitation (Figure 4F). Supplementation of PA in the culture media led to an increased binding affinity between RELA and *MARS* promoters as more immunoprecipitated promoter fragments were amplified (Figure 4F). These results indicate that PA may activate *MARS* through the NF-κB pathway.

(C) Incidence of CHD in embryos when pregnant mice were fed normal chow or fatty-acid-rich chow. Significance was calculated using a one-way ANOVA.
(D) MARS expression and K-Hcy levels in the heart tissues of mouse embryos were detected by western blotting (n = 6 per group).
(E) Homocysteine levels in the heart tissues of mouse embryos did not change in the high-PA-diet group (n = 7 per group).
(F) HTL levels in the heart tissues of mouse embryos were elevated in the high-PA-diet group (n = 7 per group).
The data are expressed as mean ± SEM. ***$p < 0.001$, **$p < 0.01$, *$p < 0.05$, non-significant (^{ns})$p > 0.05$ using unpaired Student's t tests.
See also Figure S1.

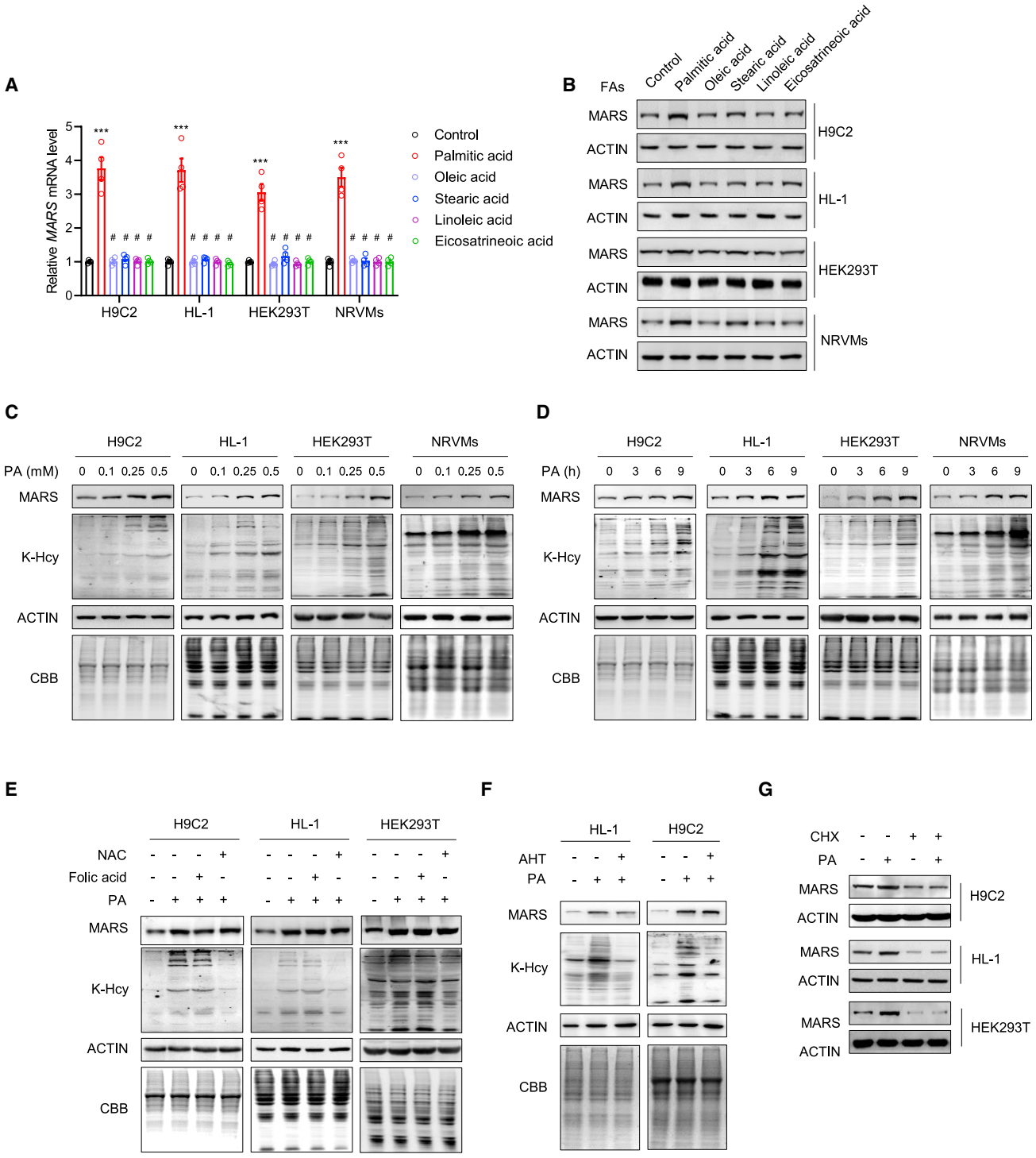

Figure 3. PA increased MARS expression and protein lysine homocysteinylation

(A and B) PA, but not other fatty acids, strongly activated *MARS* mRNA expression (A) and protein expression (B) in HL-1, H9C2, HEK293T, and NRVM cells. Cells were treated with fatty acids for 9 h before harvesting (n = 4 biological replicates per group).

(C) Elevated PA levels led to a dose-dependent increase in MARS expression in HL-1, H9C2, HEK293T, and NRVM cells. Cells were treated with PA for 9 h before harvesting. CBB, Coomassie brilliant blue.

(D) PA led to time-dependent increases in MARS expression in HL-1, H9C2, HEK293T, and NRVM cells. Cells were treated with PA (0.5 mM) for the indicated times before harvesting. CBB, Coomassie brilliant blue.

(legend continued on next page)

The NF-κB pathway was also activated in the heart tissue of embryos from pregnant mice fed a high-PA diet (Figure 4G). We also performed immunohistochemistry (IHC) analysis for heart sections and confirmed that the NF-κB pathway was activated and K-Hcy was elevated in heart tissue of embryos from pregnant mice fed a high-PA diet (Figure 4H). Taken together, these results suggest that increased PA levels enhance *MARS* transcription by activating the NF-κB pathway.

MARS promotes the K-Hcy of GATA4

We investigated the mechanisms underlying the teratogenic effects of K-Hcy on heart development. In our previous studies,[12,24] we systematically identified MARS-interacting proteins and K-Hcy-modified protein substrates. However, no transcription factors modified by K-Hcy were identified. We presumed that this was because of their low expression levels. Considering that most of the PA-correlated phenotypes in both clinical patients and the mouse models were septal defects, which were reported to be associated with genetic mutations in transcription factors belonging to families, such as GATA, TBX, and NKX, we tested the interactions between MARS and GATA4, TBX5, NKX2-5, MEF2A, and SRF.

First, we validated that MARS was located in both the cytosol and nucleus (Figure 5A). Next, we screened the potential interactions between MARS and the aforementioned transcription factors using co-immunoprecipitation assays with exogenous proteins. We found that GATA4 (Figure 5B), but not the other CHD-related transcription factors (Figure S6A), interacted with MARS. The interaction between GATA4 and MARS was confirmed by co-immunoprecipitation assays using endogenous GATA4 and MARS in cultured HL-1 cells (Figure 5C) and human ventricular septum samples from patients with CHD who had undergone surgery (Figure 5D). Moreover, the interaction between GATA4 and MARS was validated by the results of tandem affinity purification performed using GATA4 as the bait (Table S3). Our results suggest that changes in the signaling of GATA4, which is involved in septal defect pathogenesis, may contribute to the pathology associated with K-Hcy. Therefore, we used liquid chromatography followed by tandem mass spectrometry (LC-MS/MS) to screen for K-Hcy-modified sites in GATA4. We found that the lysine 300 residue of GATA4 (K300) (K299 in mice and rats) was homocysteinylated in HEK293T cells (Figure 5E). GATA4 K300 was also homocysteinylated in the cardiac tissues of embryos from high-PA-diet-fed mice (Figure S6B).

The overexpression of MARS increased the K-Hcy-modified level of GATA4 in cultured HL-1 cells (Figure 5F). However, PA did not increase the K-Hcy-modified level of GATA4 in *Mars*-knockdown HL-1 cells (Figure 5G). Moreover, the K-Hcy-modified level of GATA4 was increased in the embryos from high-PA-diet-fed mice compared with that in embryos from normal-diet-fed mice (Figure 2E). Taken together, these results confirm that PA activates MARS and leads to the increased K-Hcy modification of GATA4.

K-Hcy inactivates GATA4 and impedes its binding to promoters

We explored whether K-Hcy modification affects GATA4 function. The K300 site is evolutionarily conserved across species, from *Danio rerio* to *Homo sapiens* (Figure S6C), suggesting that K-Hcy potentially affects GATA4 function. The increased K-Hcy modification of GATA4, induced by increased PA levels, did not alter GATA4 expression at either the mRNA or protein levels (Figures S6D and S6E) and did not affect the nuclear localization of GATA4, as shown by the western blotting analysis (Figure S6F). To better evaluate GATA4 activity under different treatments, we detected the mRNA expression of well-characterized GATA4 transcription-regulated targets, including *Nppa*, *Myh7*, *Tnni3*, and *Myl1*.[27–29] The mRNA expression of these targets was significantly decreased in PA-treated HL-1 and H9C2 cells but not in *Mars*-knockdown HL-1 and H9C2 cells (Figure 6A). The deletion of GATA4 has been reported to inhibit cell proliferation,[30] and the downregulation of GATA4 causes cardiomyocyte apoptosis.[31] These effects are parallel with the anti-proliferative and pro-apoptotic roles of PA[32]; therefore, the effects of PA and MARS on cell proliferation and apoptosis were evaluated. Since PA, NF-κB, and GATA4 have all been reported to be associated with cell proliferation and apoptosis, we monitored proliferation and apoptosis in HL-1 and H9C2 cells. PA treatment decreased cell proliferation and promoted apoptosis in HL-1 and H9C2 cells, whereas the knockdown of *Mars* partially alleviated these effects (Figures S6G and S6H). Proliferation and apoptosis also accounted for the teratogenic role of PA and MARS. Moreover, in *Gata4*-knockdown HL-1 and H9C2 cells, the expressions of *Nppa*, *Myh7*, *Tnni3*, and *Myl1* decreased significantly and were no longer responsive to PA treatment (Figure 6B). In addition to *Nppa*, *Myh7*, *Tnni3*, and *Myl1*, other Gata4 downstream targets, such as *Myl3*, *Tnnc1*, and *Nppb*,[33] were generally regulated by PA in normal, but not *Gata4*-knockdown, HL-1 and H9C2 cells (Figure S6I). These results indicate that K-Hcy modification inhibits GATA4 activity.

The K300 site is located close to the GATA4 zinc-finger DNA-binding domain (amino acids 271–295), suggesting that K-Hcy modification impairs the DNA-binding affinity of GATA4 to gene promoters. By using *in vitro* EMSAs, we confirmed that GATA4 bound to the *Nppa* promoter region consisting of the GATA4-binding motif "HGATAR" (Figure 6C). However, when we increased the K-Hcy level of GATA4 by adding HTL during EMSA, the binding affinity of GATA4 for the *Nppa* promoter decreased significantly (Figure 6C). Moreover, we found that although GATA4 bound to the promoter regions of *Nppa* and *Myh7*, elevated K-Hcy levels induced by the increased PA levels in the culture media abrogated the binding of GATA4 to these promoter regions in HL-1 cells as revealed by chromatin

(E) NAC, but not folic acid, decreased pan-K-Hcy levels in PA-treated cells. The cells were treated with 0.5 mM PA, 1 mM NAC, and 100 nM folic acid for 9 h before harvesting. CBB, Coomassie brilliant blue.

(F) AHT decreased pan-K-Hcy levels in PA-treated cells. The cells were treated with 0.5 mM PA and 50 μM AHT for 9 h before harvesting.

(G) Cycloheximide (CHX) treatment blocked the effect of PA on MARS expression. Cells were treated with 200 μg/mL CHX and 0.5 mM PA for 9 h before harvesting.

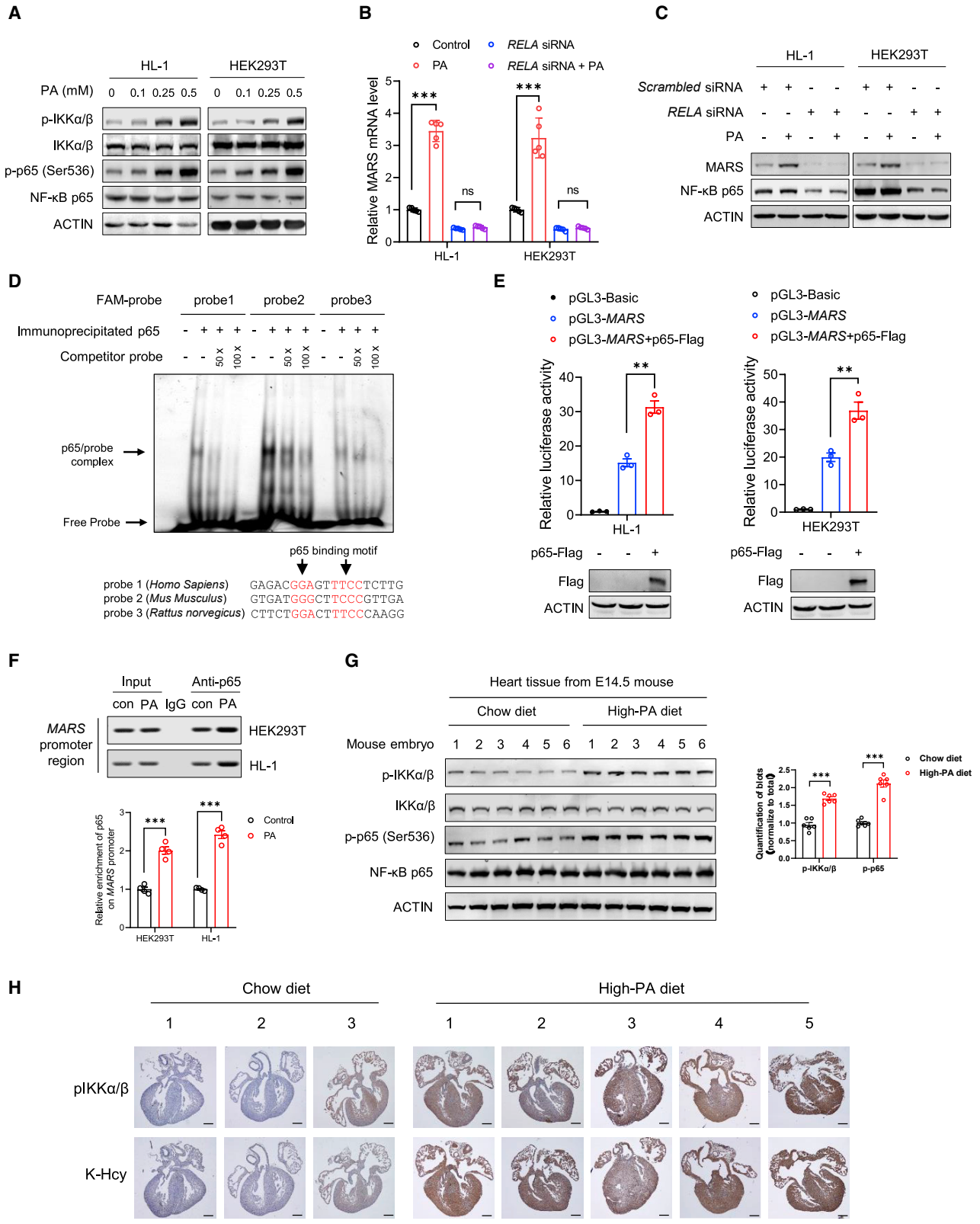

(legend on next page)

immunoprecipitation analyses (Figure 6D). Moreover, to mimic the bulky side-chain effects of K-Hcy, we created mutant constructs of GATA4 in which the modifiable lysine was mutated to tryptophan (GATA4 K300W mutant). GATA4 K300W showed diminished K-Hcy levels (Figure 6E). By using immunofluorescence staining in HL-1 cells that stably overexpressed wild-type GATA4 or the GATA4 K300W mutant, we found that the K300W mutant did not exhibit altered nuclear localization (Figure S6J). The EMSAs validated that the binding affinity of the GATA4 K300W mutant to the gene promoter was weaker than that of the wild-type GATA4 (Figure 6F). This notion was further confirmed by the lower expression levels of the downstream targets of GATA4 when overexpressing the GATA4 K300W mutant compared with overexpressing wild-type GATA4 (Figure 6G). By rescuing wild-type GATA4 and GATA4 K300W in sh*GATA4* HL-1 and H9C2 cells combined with PA treatment, we found that PA suppressed cardiac gene expression in sh*GATA4*+GATA4 wild-type cells. PA treatment did not suppress cardiac gene expression in sh*GATA4*+GATA4 K300W cells, suggesting that K300 was essential for PA-mediated cardiac gene suppression (Figure 6G). These results confirmed that the K-Hcy modification of GATA4 inhibited GATA4 transcriptional activity.

Reduced GATA4 function has previously been reported to be associated with a bias toward endothelial cell fate.[34] Therefore, we tested the expressions of the core transcription regulators of endothelial cells (SOX17) and ETS factors (ETS1) in heart tissues from the embryos of high-PA-diet-fed mice. The expressions of SOX17 and ETS1 were increased (Figure 2E), suggesting that endothelial/endocardial programs were upregulated. These phenomena could also provide an explanation for PA-induced CHDs.

Blocking K-Hcy rescues GATA4 function and decreases CHD prevalence in mice with high levels of PA

To further confirm that gestational PA induces CHD in offspring by activating MARS and K-Hcy, we investigated whether depleting MARS could block the teratogenic effects of PA. Eight-week-old wild-type female mice were mated with 8-week-old *Mars* heterozygous knockout male mice. Pregnant mice were administered high-PA chow from E0.5–E13.5. The cardiac phenotypes of the embryos at E14.5 were examined using histological analyses, and their genotypes were tested using PCR. We found that although high-PA chow induced the occurrence of CHD phenotypes, the incidence of CHD was lower in *Mars* heterozygous knockout embryos than in wild-type embryos (Figure 7A). The results show that the cardiac K-Hcy of GATA4 decreased; the cardiac expression levels of the downstream targets of GATA4 increased; and the endothelial/endocardial regulators decreased in *Mars* heterozygous knockout embryos compared with those in wild-type embryos (Figure 7B). Blocking the activation of MARS therefore rescued the teratogenic effects of PA. These findings indicate a potential strategy for preventing high-PA-induced CHD occurrence when MARS is overactivated.

NAC and AHT can inhibit MARS activity and decrease K-Hcy levels in cultured cells. We found that supplementation with NAC and AHT, but not folic acid, decreased the K-Hcy-modified level of GATA4 and abrogated the effect of PA treatment in cultured HL-1 and HEK293T cells (Figures 7C and S7A). In addition, NAC or AHT supplementation increased the expressions of the downstream targets of GATA4 in PA-treated HL-1 and HEK293T cells (Figures 7D and S7B). NAC also alleviated PA-induced apoptosis and the inhibition of proliferation (Figures S7C and S7D). In the high-PA-diet-fed mice, a daily dose of 300 mg/kg NAC, administered from E0.5 to the end of the experiment, significantly decreased the high-PA-diet-induced incidence of CHD. The percentage of pregnant mice bearing offspring with CHD decreased significantly (Figures 7E and 7F), whereas the incidence of CHD in embryos decreased from 29.33% (22 in 75) to 8.64% (7 in 81; Figure 7F). Notably, NAC decreased the levels of GATA4 and activated GATA4 in the embryonic hearts of offspring obtained from high-PA-diet-fed mice (Figure 7G). In contrast, folic acid supplementation during pregnancy did not rescue the above phenotypes caused by high-PA-chow feeding, including the increased K-Hcy modification of GATA4, decreased expression levels of GATA4-regulated targets, increased expression levels of endothelial/endocardial regulators, and increased incidence of CHD in embryos (Figures 7E and 7F). These findings suggest that PA promotes K-Hcy by activating MARS expression and blocking the response to folic acid. This indicates that the inhibition of MARS-mediated signaling under increased circulating PA levels can be used to prevent CHD (Figure 7G).

DISCUSSION

Using clinical samples and *in vitro* and *in vivo* models, we showed that increased maternal PA levels amplified teratogenic K-Hcy signals by activating *MARS* transcription. Increased K-Hcy inhibited embryonic GATA4 signaling and increased the

Figure 4. PA increases *MARS* transcription by activating the NF-κB pathway

(A) PA activated the NF-κB pathway in cultured HEK293T and HL-1 cells. Cells were treated with PA for 4 h before harvesting.

(B) Knockdown of *RELA* blocked the effect of PA on *MARS* mRNA expression (n = 5 biological replicates per group).

(C) Knockdown of *RELA* blocked the effect of PA on activating MARS protein expression.

(D) EMSAs showed RELA bound to the *MARS* promoter region in three species.

(E) Effects of p65 on the transcription activities of the human *MARS* promoter in HEK293T cells and mouse *Mars* promoter in HL-1 cells, determined using dual-luciferase reporter assays (n = 3 biological replicates per group).

(F) Chromatin immunoprecipitation (ChIP)-PCR (top) and ChIP-qPCR (bottom) assays were performed using p65 antibody in both HL-1 and HEK293T cells untreated or treated with PA. Rabbit immunoglobulin G (IgG) antibody was used as the control (n = 4 per group).

(G) The NF-κB pathway was activated in the embryonic heart tissue of maternal high-PA-chow-fed mice, as detected by western blotting (n = 6 mice per group).

(H) IHC staining of pIKKa/β and K-Hcy for embryonic heart sections of mice model. Scale bar, 500 μm (n = 3 mice for chow-diet group, n = 5 mice for high-PA group).

The data are expressed as mean ± SEM. ***$p < 0.001$, **$p < 0.01$, *$p < 0.05$, $^{ns}p > 0.05$ using unpaired Student's t tests.

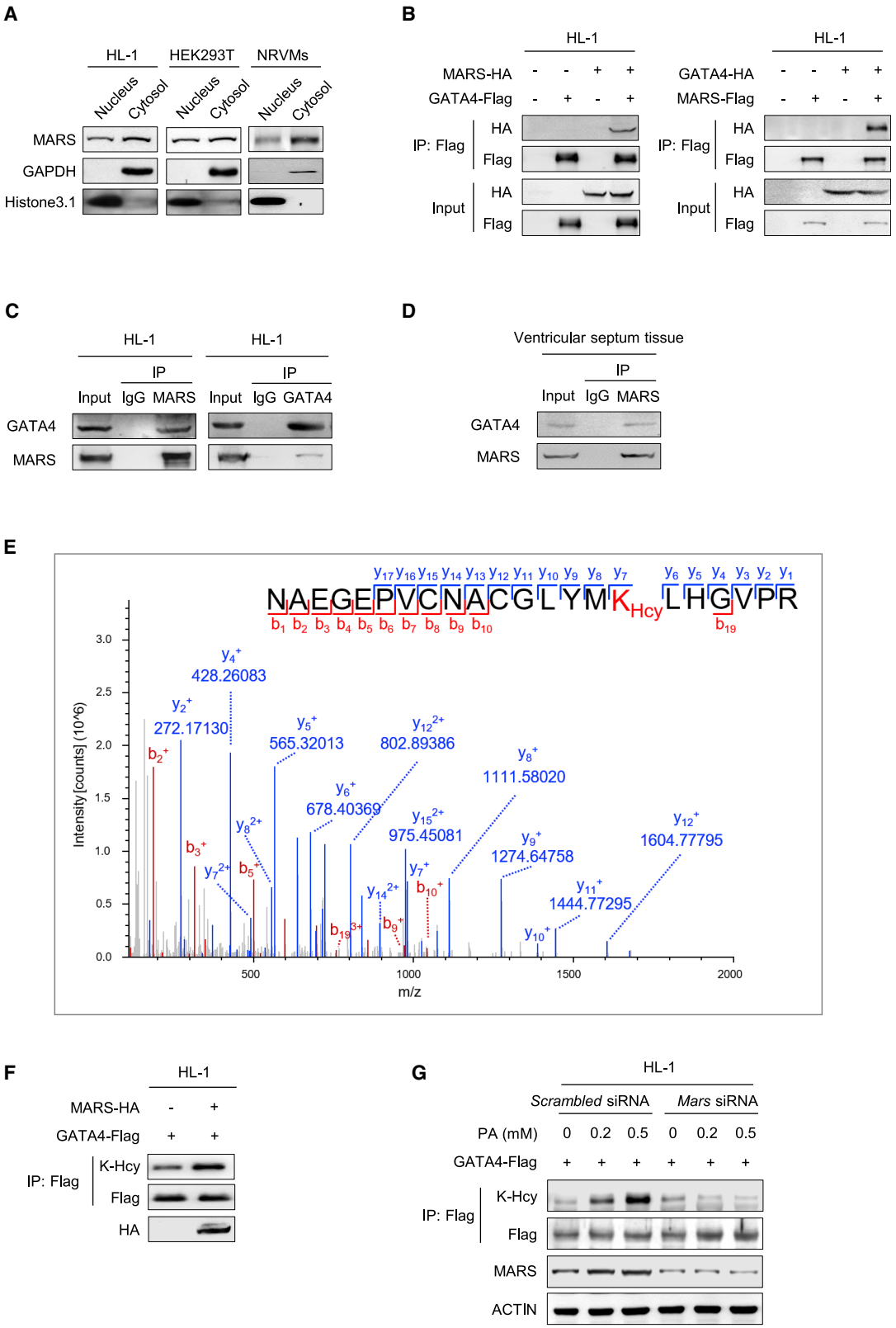

(legend on next page)

risk of CHD in the offspring. Although we did not determine the levels of PA in the earlier stages of pregnancy, the teratogenic effects of PA were evident in our mouse model. This suggested that increased maternal circulating PA levels from E0.5–E13.5, which included the entire period required for embryonic heart development, led to an elevated risk of CHD in the offspring. We also found that increased maternal PA levels did not induce the onset of CHD in *Mars*-knockout mice, confirming that PA exerted its teratogenic effects via MARS-mediated K-Hcy signaling.

The K-Hcy modification of proteins, which was determined by both homocysteine concentrations and MARS protein levels, caused the onset of CHD. Our findings indicate that PA activates *MARS* transcription, suggesting that high maternal levels of PA may abrogate the protective effect of folic acid, as the PA-induced elevation of K-Hcy does not require high levels of homocysteine. That is, under normal PA levels, MARS proceeds normally in translation, and the K-Hcy level is determined by the intracellular homocysteine concentration; hence, both K-Hcy and homocysteine respond to folate or folic acid levels. However, when PA levels are high, the expression of MARS increases, thereby markedly increasing the efficiency of K-Hcy formation. Under these conditions, supplementation with folic acid did not reduce protein K-Hcy. Accordingly, in our high-PA-diet-fed mouse model, the inhibition of MARS, but not supplementation of folic acid, could rescue all the pathological effects caused by PA (see Figure 7).

We have previously conducted a cell-wide proteomics survey and identified K-Hcy-modified proteins.[12] However, no transcription factors associated with the K-Hcy modification of proteins have been identified, possibly because of the low protein density of transcription factors in cells. Because defects in transcription factors are known to be the principal cause of CHD, we hypothesized that CHD-related transcription factors are affected by K-Hcy. We found that GATA4 was heavily modified by K-Hcy. GATA4 plays a crucial role in the regulation of heart development, which has been shown in several studies, as best evidenced by the fact that GATA4 mutations are associated with numerous congenital septal defects in humans.[34–39] GATA4 has the ability to bind through its zinc-finger DNA-binding domain and sequence-specific DNA motifs and regulate the transcription of target genes. We found a homocysteinylated lysine residue located close to the GATA4 zinc-finger DNA-binding domain and found that K-Hcy modification abrogated the DNA-binding affinity of GATA4. These results indicated that, in addition to genetic mutations, post-translational modifications also led to the inactivation of GATA4 and the onset of CHD. As we did not obtain proteome-wide K-Hcy-modified transcription factors, it is possible that K-Hcy modifies and affects proteins other than GATA4 that are involved in septal defects. Elevated oxidative stress is also an important factor involved in PA and K-Hcy-induced CHD onset, and reactive oxygen species is widely acknowledged as a risk factor for multiple developmental defects, including incorrect implantation of embryos, miscarriages, premature births, low birth weight, and malformations.[40,41] In this study, we found that K-Hcy regulates GATA4 activity, which further demonstrates how K-Hcy specifically contributes to cardiac dysplasia and septal defects.

Our study found that increased maternal PA levels caused VSD and ASD phenotypes in mice, which was in accordance with the maternal hyperhomocysteine-induced and GATA4 mutation-induced CHD phenotypes in humans.[42–46] These phenomena suggest that PA signals have a crosstalk with homocysteine signals and synergistically regulate GATA4 signals. Besides septal defects, GATA4 mutations have also been reported to be associated with complex CHDs. A study has further revealed that GATA4 is a dose-sensitive regulator of cardiac morphogenesis.[47] Embryos expressing 70% less GATA4 protein had a common atrioventricular canal (CAVC), double outlet right ventricle (DORV), hypoplastic ventricular myocardium, and normal coronary vasculature and died between embryonic day E13.5 and E16.5, whereas embryos expressing 50% less GATA4 protein survived normally. Besides regulating embryonic heart development, GATA4 plays a key role in postnatal cardiac structural remodeling, as loss-of-function mutations of GATA4 were reported to be responsible for familial dilated cardiomyopathy,[48] sporadic dilated cardiomyopathy,[49] familial atrial fibrillation,[50] and lone atrial fibrillation.[51] It will be interesting to explore the connection between nutrient signals and GATA4 function in cardiac remodeling in the future. In this study, we did not observe additional CHD phenotypes, such as CAVC or DORV, as PA only partially inhibited GATA4 activity. As for the relationship between fatty acids and CHD, a previous study showed that maternal type 2 diabetes, which was induced by a 15-week high-fat diet, significantly induced septal defects and persistent truncus arteriosus in the development heart of the offspring, along with increased oxidative stress and apoptosis in the embryonic heart.[21] However, few mutations in the genes necessary for fatty acid metabolism have been found in patients with CHD. In a case report,[52] a patient with a multiple acyl-coenzyme A (CoA) dehydrogenase deficiency (glutaric aciduria type II [GAII]), which is a deficiency in the electron transfer flavoprotein and leads to the accumulation of FFAs in the plasma, was born with ASD and VSD. These results indicate that exogenous FFA signals from the diet may be much more important than inborn fatty acid metabolic abnormalities.

In conclusion, we found that increased levels of maternal PA increased the risk of CHD in offspring by inhibiting GATA4 signaling in embryos through the NF-κB-MARS-K-Hcy pathway.

Figure 5. MARS promotes lysine-homocysteinylation of GATA4

(A) MARS is located in both the cytosol and nuclei of HL-1, HEK239T, and NRVM cells.

(B) Co-immunoprecipitation assays showed that exogenous MARS interacted with exogenous GATA4 in cultured HL-1 cells.

(C and D) Co-immunoprecipitation assays showed that endogenous MARS interacted with endogenous GATA4 in cultured HL-1 cells (C) and human heart tissue (D).

(E) GATA4 K300 was homocysteinylated, as determined by LC-MS/MS. The MS/MS spectrum of the peptide is shown.

(F) MARS overexpression enhanced the K-Hcy modification of GATA4 in HL-1 cells.

(G) PA did not increase the K-Hcy-modified level of GATA4 in *MARS*-knockdown HL-1 cells.

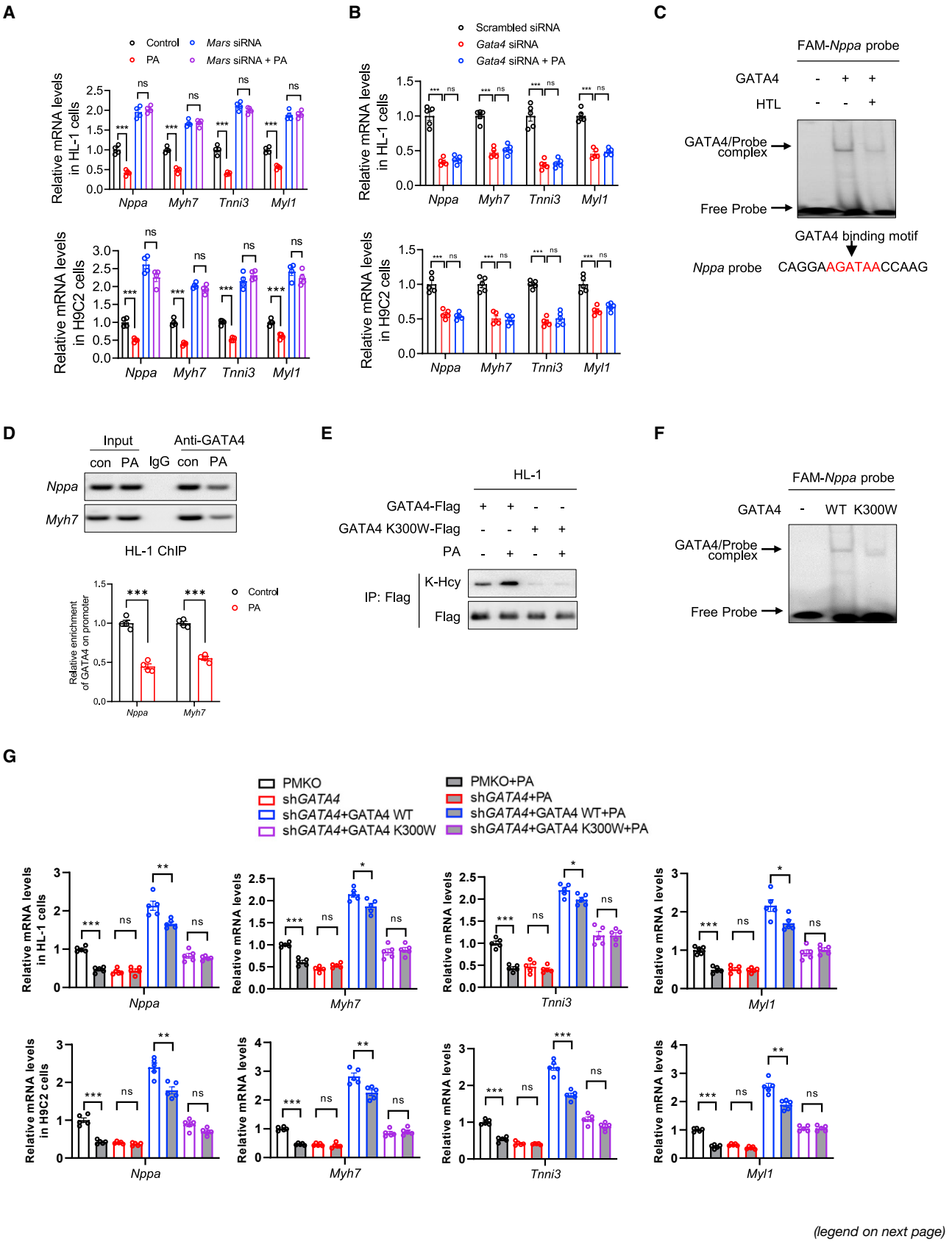

(legend on next page)

The inhibition of MARS prevented the PA-induced elevation of K-Hcy in the embryonic heart and decreased the risk of CHD in the offspring, highlighting the potential use of targeting this pathway for the prevention and treatment of CHD.

Limitations of the study

When analyzing fatty acids levels from clinical samples, we did not collect cord blood, which is a direct link between mother and offspring, and detecting metabolic changes in cord blood may better interpret the influence to offspring from mother. K-Hcy modification affects numerous substrates such as histones that will influence embryonic development.[53] In this study, we found that PA also increased total K-Hcy levels of histones in fetus heart tissue (Figure S7E), which contributed to the pathogenic role of PA/K-Hcy-induced CHD. The functions of K-Hcy on histones need to be further studied. AHT was previously reported[12] to inhibit CHD incidence induced by all-*trans* retinoic acid in mice and chicken embryos by inhibiting K-Hcy, and if AHT could rescue PA-induced CHD warrants further validation.

STAR★METHODS

Detailed methods are provided in the online version of this paper and include the following:

- KEY RESOURCES TABLE
- RESOURCE AVAILABILITY
  - Lead contact
  - Materials availability
  - Data and code availability
- EXPERIMENTAL MODEL AND SUBJECT DETAILS
  - Study participants
  - Animal models
  - Cell lines
  - Neonatal rat ventricular myocytes culture
- METHOD DETAILS
  - Physiological index evaluation of the experimental animals
  - Mouse embryo heart isolation and histological analysis
  - Immunohistochemistry
  - Quantification of metabolites in the plasma
  - Gas chromatography coupled to either a flame ionization detector or mass spectrometer analysis of fatty acids
  - Plasmid constructs
  - Nuclei and histone isolation
  - Immunoprecipitation and western blotting
  - Preparation of K-Hcy antibody
  - RNA extraction and quantitative real-time PCR
  - Dual-luciferase reporter assay
  - Electrophoretic mobility shift assay
  - Chromatin immunoprecipitation (ChIP) assay
  - RNAi
  - Sample preparation for LC-MS/MS analysis
  - LC-MS/MS analysis
  - K-Hcy site identification
  - Hcy and HTL quantification
  - Cell proliferation and apoptosis assay
  - Immunofluorescence
- QUANTIFICATION AND STATISTICAL ANALYSIS

SUPPLEMENTAL INFORMATION

Supplemental information can be found online at https://doi.org/10.1016/j.xcrm.2023.100953.

ACKNOWLEDGMENTS

This work was supported by grants from National Key R&D Program of China (nos. 2020YFA0803601 and 2019YFA0801900), the fellowship of China Postdoctoral Science Foundation (2020M670987), and the National Natural Science Foundation of China (nos. 82130015, 31871432, 81771627, 81971061, 81770312, 81970572, and 32000895). Objects in graphical abstract were acquired from Figdraw (www.figdraw.com, ID: 533420148).

AUTHOR CONTRIBUTIONS

J.-Y.Z., K.S., J.C., and X.-Y.Z. conceived of the presented idea. R.Z., L.C., W.-J.G., L.L., Z.-Z.C., and J.C. performed the experiments. J.X., Z.-Y.Z., and W.-D.Z. assisted with the experiments. R.Z., Z.-Z.C., X.-Y.Z., and J.C. performed the analysis. J.-Y.Z. and R.Z. drafted the manuscript. All authors discussed the results and commented on the manuscript.

DECLARATION OF INTERESTS

The authors declare no competing interests.

Received: August 12, 2022
Revised: December 13, 2022
Accepted: January 31, 2023
Published: February 20, 2023

Figure 6. K-Hcy inactivates GATA4 and impedes its binding to the promoter

(A) PA treatment decreased the mRNA levels of GATA4 downstream targets (*Nppa*, *Myh7*, *Tnni3*, and *Myl1*) in HL-1 (top) and H9C2 cells (bottom), and this effect was abolished in *Mars*-knockdown cells (n = 4 biological replicates per group).

(B) PA did not decrease the mRNA levels of GATA4 downstream targets in *Gata4*-knockdown HL-1 (top) and H9C2 (bottom) cells (n = 4 biological replicates per group).

(C) EMSAs showed that HTL decreased the binding affinity of GATA4 for the *Nppa* probe. The sequence of the FAM-labeled probe was obtained from the *Mus Musculus Nppa* promoter.

(D) ChIP-PCR (top) and ChIP-qPCR (bottom) assays showed that PA decreased the binding of GATA4 to the *Mus musculus Nppa* and *Myh7* promoters (n = 5 biological replicates per group).

(E) K-Hcy levels in exogenous wild-type GATA4 and GATA4 K300W mutants.

(F) The EMSA showed that the GATA4 K300W mutant exhibited a lower binding affinity for the *Nppa* probe than wild-type GATA4.

(G) Overexpression of wild-type GATA4, but not K300W, rescued the effect of PA-mediated cardiac gene suppression in sh*GATA4* HL-1 and H9C2 cells (n = 4 biological replicates per group).

The data are expressed as mean ± SEM. ***$p < 0.001$, **$p < 0.01$, *$p < 0.05$, $^{ns}p > 0.05$ using unpaired Student's t tests.

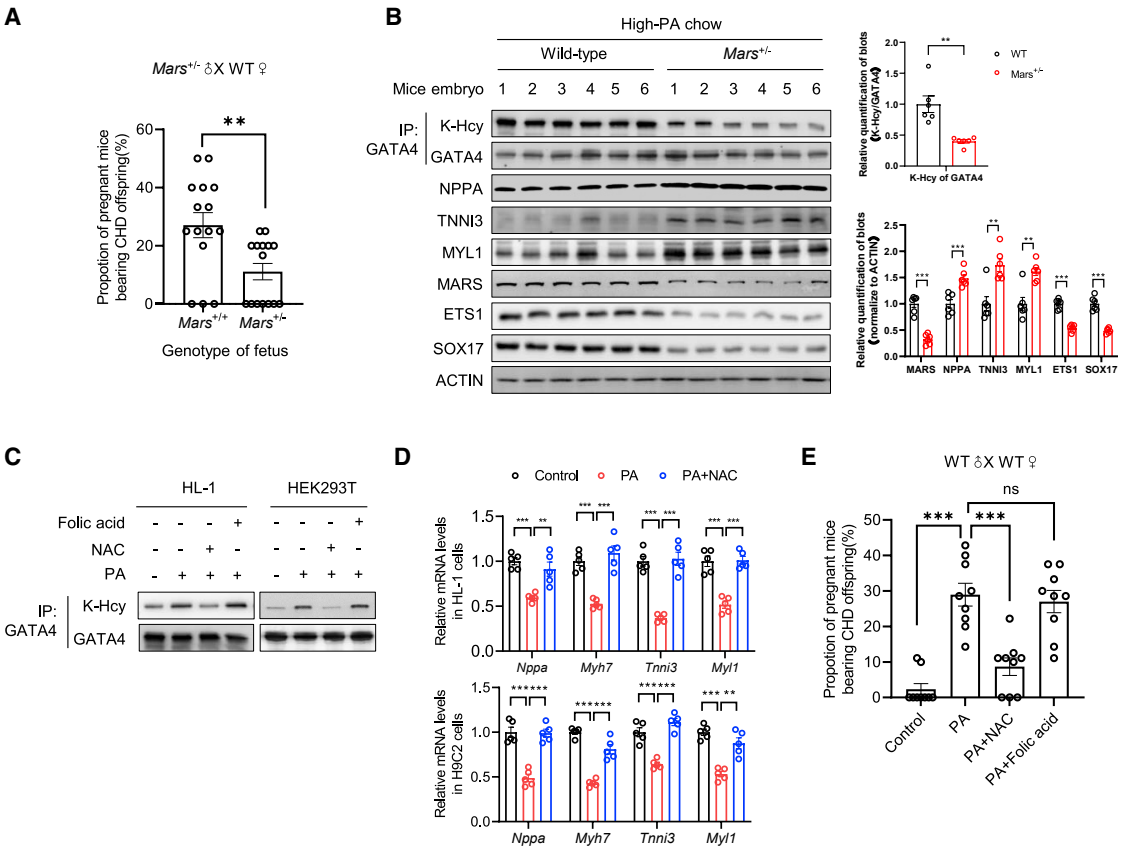

F

Incidence of CHD embryos

	Group	Pregnant mice	Total fetuses	Absorbed fetuses	VSD	ASD	Ratio of CHD	*p* value	RR (95%CI)
WT ♂ X WT ♀	Control	9	80	2	1	1	2.56%	/	/
	PA	9	80	5	12	10	29.33%	5.3×10^{-6} (***)	11.44 (2.79-46.97)
	PA+NAC	9	83	2	4	3	8.64%	0.19 (ns)	3.37 (0.72-15.73)
	PA+Folic acid	9	77	3	9	11	27.03%	1.8×10^{-5} (***)	10.54 (2.55-43.53)
Mars$^{+/-}$ ♂ X WT ♀ High-PA diet	*Mars*$^{+/+}$	15	66	3	9	8	26.98%	/	/
	Mars$^{+/-}$		72	2	4	4	11.43%	0.02 (*)	0.42 (0.20-0.91)

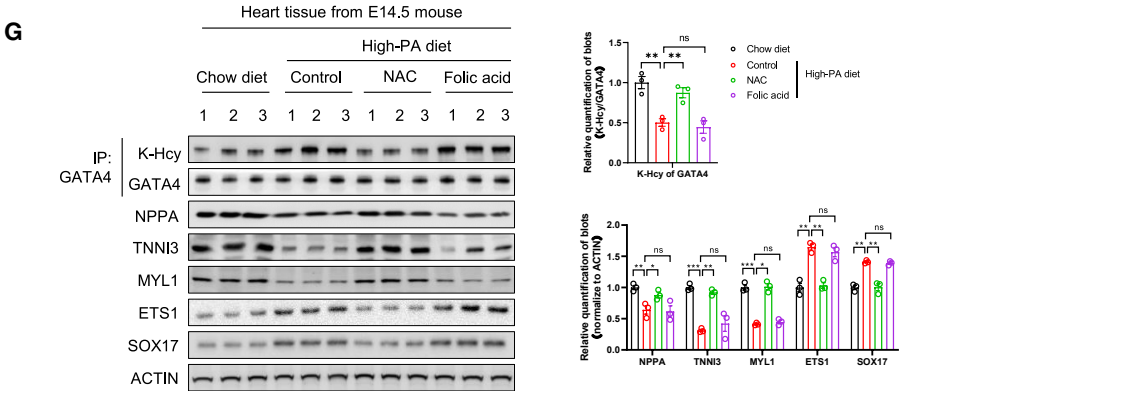

(legend on next page)

REFERENCES

1. van der Linde, D., Konings, E.E.M., Slager, M.A., Witsenburg, M., Helbing, W.A., Takkenberg, J.J.M., and Roos-Hesselink, J.W. (2011). Birth prevalence of congenital heart disease worldwide: a systematic review and meta-analysis. J. Am. Coll. Cardiol. *58*, 2241–2247. https://doi.org/10.1016/j.jacc.2011.08.025.
2. Botto, L.D., and Correa, A. (2003). Decreasing the burden of congenital heart anomalies: an epidemiologic evaluation of risk factors and survival. Prog. Pediatr. Cardiol. *18*, 111–121. https://doi.org/10.1016/s1058-9813(03)00084-5.
3. Botto, L.D., Mulinare, J., and Erickson, J.D. (2003). Do multivitamin or folic acid supplements reduce the risk for congenital heart defects? Evidence and gaps. Am. J. Med. Genet. *121a*, 95–101.
4. Feng, Y., Wang, S., Chen, R., Tong, X., Wu, Z., and Mo, X. (2015). Maternal folic acid supplementation and the risk of congenital heart defects in offspring: a meta-analysis of epidemiological observational studies. Sci. Rep. *5*, 8506. https://doi.org/10.1038/srep08506.
5. Botto, L.D., Mulinare, J., and Erickson, J.D. (2000). Occurrence of congenital heart defects in relation to maternal multivitamin use. Am. J. Epidemiol. *151*, 878–884.
6. Hernández-Díaz, S., Werler, M.M., Walker, A.M., and Mitchell, A.A. (2000). Folic acid antagonists during pregnancy and the risk of birth defects. N. Engl. J. Med. *343*, 1608–1614. https://doi.org/10.1056/NEJM200011303432204.
7. Zhao, J.Y., Yang, X.Y., Gong, X.H., Gu, Z.Y., Duan, W.Y., Wang, J., Ye, Z.Z., Shen, H.B., Shi, K.H., Hou, J., et al. (2012). Functional variant in methionine synthase reductase intron-1 significantly increases the risk of congenital heart disease in the han Chinese population. Circulation *125*, 482–490.
8. Zhao, J.Y., Yang, X.Y., Shi, K.H., Sun, S.N., Hou, J., Ye, Z.Z., Wang, J., Duan, W.Y., Qiao, B., Chen, Y.J., et al. (2013). A functional variant in the cystathionine beta-synthase gene promoter significantly reduces congenital heart disease susceptibility in a Han Chinese population. Cell Res. *23*, 242–253. https://doi.org/10.1038/cr.2012.135.
9. Zhao, J.Y., Qiao, B., Duan, W.Y., Gong, X.H., Peng, Q.Q., Jiang, S.S., Lu, C.Q., Chen, Y.J., Shen, H.B., Huang, G.Y., et al. (2014). Genetic variants reducing MTR gene expression increase the risk of congenital heart disease in Han Chinese populations. Eur. Heart J. *35*, 733–742. https://doi.org/10.1093/eurheartj/eht221.
10. Wang, D., Wang, F., Shi, K.H., Tao, H., Li, Y., Zhao, R., Lu, H., Duan, W., Qiao, B., Zhao, S.M., et al. (2017). Lower circulating folate induced by a fidgetin intronic variant is associated with reduced congenital heart disease susceptibility. Circulation *135*, 1733–1748. https://doi.org/10.1161/CIRCULATIONAHA.116.025164.
11. Jakubowski, H. (2019). Homocysteine modification in protein structure/function and human disease. Physiol. Rev. *99*, 555–604. https://doi.org/10.1152/physrev.00003.2018.
12. Mei, X., Qi, D., Zhang, T., Zhao, Y., Jin, L., Hou, J., Wang, J., Lin, Y., Xue, Y., Zhu, P., et al. (2020). Inhibiting MARSs reduces hyperhomocysteinemia-associated neural tube and congenital heart defects. EMBO Mol. Med. *12*, e9469. https://doi.org/10.15252/emmm.201809469.
13. Jakubowski, H., Zhang, L., Bardeguez, A., and Aviv, A. (2000). Homocysteine thiolactone and protein homocysteinylation in human endothelial cells: implications for atherosclerosis. Circ. Res. *87*, 45–51. https://doi.org/10.1161/01.res.87.1.45.
14. Correa, A., and Marcinkevage, J. (2013). Prepregnancy obesity and the risk of birth defects: an update. Nutr. Rev. *71*, S68–S77. https://doi.org/10.1111/nure.12058.
15. Stothard, K.J., Tennant, P.W.G., Bell, R., and Rankin, J. (2009). Maternal overweight and obesity and the risk of congenital anomalies: a systematic review and meta-analysis. JAMA *301*, 636–650. https://doi.org/10.1001/jama.2009.113.
16. Persson, M., Razaz, N., Edstedt Bonamy, A.K., Villamor, E., and Cnattingius, S. (2019). Maternal overweight and obesity and risk of congenital heart defects. J. Am. Coll. Cardiol. *73*, 44–53. https://doi.org/10.1016/j.jacc.2018.10.050.
17. Cai, G.J., Sun, X.X., Zhang, L., and Hong, Q. (2014). Association between maternal body mass index and congenital heart defects in offspring: a systematic review. Am. J. Obstet. Gynecol. *211*, 91–117. https://doi.org/10.1016/j.ajog.2014.03.028.
18. Nederlof, M., de Walle, H.E.K., van Poppel, M.N.M., Vrijkotte, T.G.M., and Gademan, M.G.J. (2015). Deviant early pregnancy maternal triglyceride levels and increased risk of congenital anomalies: a prospective community-based cohort study. BJOG *122*, 1176–1183. https://doi.org/10.1111/1471-0528.13393.
19. Smedts, H.P.M., Rakhshandehroo, M., Verkleij-Hagoort, A.C., de Vries, J.H.M., Ottenkamp, J., Steegers, E.A.P., and Steegers-Theunissen, R.P.M. (2008). Maternal intake of fat, riboflavin and nicotinamide and the risk of having offspring with congenital heart defects. Eur. J. Nutr. *47*, 357–365.
20. Mdaki, K.S., Larsen, T.D., Wachal, A.L., Schimelpfenig, M.D., Weaver, L.J., Dooyema, S.D.R., Louwagie, E.J., and Baack, M.L. (2016). Maternal high-fat diet impairs cardiac function in offspring of diabetic pregnancy through metabolic stress and mitochondrial dysfunction. Am. J. Physiol. Heart Circ. Physiol. *310*, H681–H692.
21. Wu, Y., Reece, E.A., Zhong, J., Dong, D., Shen, W.B., Harman, C.R., and Yang, P. (2016). Type 2 diabetes mellitus induces congenital heart defects in murine embryos by increasing oxidative stress, endoplasmic reticulum stress, and apoptosis. Am. J. Obstet. Gynecol. *215*, 366.e1–366.e10, ARTN 366.e1-e10. https://doi.org/10.1016/j.ajog.2016.03.036.
22. Innis, S.M. (2007). Fatty acids and early human development. Early Hum. Dev. *83*, 761–766. https://doi.org/10.1016/j.earlhumdev.2007.09.004.
23. Chirala, S.S., Chang, H., Matzuk, M., Abu-Elheiga, L., Mao, J., Mahon, K., Finegold, M., and Wakil, S.J. (2003). Fatty acid synthesis is essential in embryonic development: fatty acid synthase null mutants and most of the

Figure 7. Blocking K-Hcy rescues GATA4 function and decreases CHD prevalence in mice with high PA levels

(A) *Mars* heterozygous knockout embryos exhibited decreased CHD incidence compared with wild-type embryos (n = 15 per group).

(B) K-Hcy levels of endogenous GATA4, protein levels of GATA4 downstream targets (NPPA, TNNI3, and MYL1), and endocardial/endothelial factors (ETS1 and SOX17) in the heart tissues of wild-type and $Mars^{+/-}$ embryonic mice. The quantification of blots is shown on the right (n = 6 mice per group).

(C) NAC, but not folic acid, decreased the levels of endogenous GATA4 in HL-1 and HEK293T cells. Cells were treated with 0.5 mM PA, 1 mM NAC, and 100nM folic acid for 9 h before harvesting.

(D) NAC increased the mRNA levels of GATA4 downstream targets in PA-treated HL-1 and HEK293T cells (n = 5 per group). Cells were treated with 0.5 mM PA and 1 mM NAC for 9 h before harvesting.

(E) NAC, but not folic acid, decreased PA-induced CHD incidence (n = 9 mice per group).

(F) Incidence of CHD in embryos from the indicated groups of pregnant mice. Significance was calculated using a one-way ANOVA.

(G) K-Hcy levels of endogenous GATA4, protein levels of GATA4 downstream targets (NPPA, TNNI3, and MYL1), and endocardial/endothelial factors (ETS1 and SOX17) in the heart tissues of embryonic mice with the indicated treatment. The quantification of blots is shown on the right (n = 3 mice per group).

The data are expressed as mean ± SEM. ***$p < 0.001$, **$p < 0.01$, *$p < 0.05$, $^{ns}p > 0.05$ using unpaired Student's t tests.

heterozygotes die in utero. Proc. Natl. Acad. Sci. USA *100*, 6358–6363. https://doi.org/10.1073/pnas.0931394100.

24. Wang, D., Zhao, R., Qu, Y.Y., Mei, X.Y., Zhang, X., Zhou, Q., Li, Y., Yang, S.B., Zuo, Z.G., Chen, Y.M., et al. (2018). Colonic lysine homocysteinylation induced by high-fat diet suppresses DNA damage repair. Cell Rep. *25*, 398–412.e6. https://doi.org/10.1016/j.celrep.2018.09.022.
25. Siddeek, B., Mauduit, C., Chehade, H., Blin, G., Liand, M., Chindamo, M., Benahmed, M., and Simeoni, U. (2019). Long-term impact of maternal high-fat diet on offspring cardiac health: role of micro-RNA biogenesis. Cell Death Dis. *5*, 71. https://doi.org/10.1038/s41420-019-0153-y.
26. Quan, J., Liu, J., Gao, X., Liu, J., Yang, H., Chen, W., Li, W., Li, Y., Yang, W., and Wang, B. (2014). Palmitate induces interleukin-8 expression in human aortic vascular smooth muscle cells via Toll-like receptor 4/nuclear factor-kappaB pathway (TLR4/NF-kappaB-8). J. Diabetes *6*, 33–41. https://doi.org/10.1111/1753-0407.12073.
27. Molkentin, J.D. (2000). The zinc finger-containing transcription factors GATA-4, -5, and -6. Ubiquitously expressed regulators of tissue-specific gene expression. J. Biol. Chem. *275*, 38949–38952. https://doi.org/10.1074/jbc.R000029200.
28. Bisping, E., Ikeda, S., Sedej, M., Wakula, P., McMullen, J.R., Tarnavski, O., Sedej, S., Izumo, S., Pu, W.T., and Pieske, B. (2012). Transcription factor GATA4 is activated but not required for insulin-like growth factor 1 (IGF1)-induced cardiac hypertrophy. J. Biol. Chem. *287*, 9827–9834. https://doi.org/10.1074/jbc.M111.338749.
29. Liang, Q., and Molkentin, J.D. (2002). Divergent signaling pathways converge on GATA4 to regulate cardiac hypertrophic gene expression. J. Mol. Cell. Cardiol. *34*, 611–616. https://doi.org/10.1006/jmcc.2002.2011.
30. Kohlnhofer, B.M., Thompson, C.A., Walker, E.M., and Battle, M.A. (2016). GATA4 regulates epithelial cell proliferation to control intestinal growth and development in mice. Cell. Mol. Gastroenterol. Hepatol. *2*, 189–209. https://doi.org/10.1016/j.jcmgh.2015.11.010.
31. Bisping, E., Ikeda, S., Kong, S.W., Tarnavski, O., Bodyak, N., McMullen, J.R., Rajagopal, S., Son, J.K., Ma, Q., Springer, Z., et al. (2006). Gata4 is required for maintenance of postnatal cardiac function and protection from pressure overload-induced heart failure. Proc. Natl. Acad. Sci. USA *103*, 14471–14476. https://doi.org/10.1073/pnas.0602543103.
32. Yang, L., Guan, G., Lei, L., Liu, J., Cao, L., and Wang, X. (2019). Oxidative and endoplasmic reticulum stresses are involved in palmitic acid-induced H9c2 cell apoptosis. Biosci. Rep. *39*. https://doi.org/10.1042/BSR20190225.
33. Misra, C., Sachan, N., McNally, C.R., Koenig, S.N., Nichols, H.A., Guggilam, A., Lucchesi, P.A., Pu, W.T., Srivastava, D., and Garg, V. (2012). Congenital heart disease-causing Gata4 mutation displays functional deficits in vivo. PLoS Genet. *8*, e1002690. https://doi.org/10.1371/journal.pgen.1002690.
34. Ang, Y.S., Rivas, R.N., Ribeiro, A.J.S., Srivas, R., Rivera, J., Stone, N.R., Pratt, K., Mohamed, T.M.A., Fu, J.D., Spencer, C.I., et al. (2016). Disease model of GATA4 mutation reveals transcription factor cooperativity in human cardiogenesis. Cell *167*, 1734–1749.e22. https://doi.org/10.1016/j.cell.2016.11.033.
35. Okubo, A., Miyoshi, O., Baba, K., Takagi, M., Tsukamoto, K., Kinoshita, A., Yoshiura, K., Kishino, T., Ohta, T., Niikawa, N., and Matsumoto, N. (2004). A novel GATA4 mutation completely segregated with atrial septal defect in a large Japanese family. J. Med. Genet. *41*, e97. https://doi.org/10.1136/jmg.2004.018895.
36. Sarkozy, A., Conti, E., Neri, C., D'Agostino, R., Digilio, M.C., Esposito, G., Toscano, A., Marino, B., Pizzuti, A., and Dallapiccola, B. (2005). Spectrum of atrial septal defects associated with mutations of NKX2.5 and GATA4 transcription factors. J. Med. Genet. *42*, e16. https://doi.org/10.1136/jmg.2004.026740.
37. Wang, J., Fang, M., Liu, X.Y., Xin, Y.F., Liu, Z.M., Chen, X.Z., Wang, X.Z., Fang, W.Y., Liu, X., and Yang, Y.Q. (2011). A novel GATA4 mutation responsible for congenital ventricular septal defects. Int. J. Mol. Med. *28*, 557–564. https://doi.org/10.3892/ijmm.2011.715.
38. Yang, Y.Q., Wang, J., Liu, X.Y., Chen, X.Z., Zhang, W., and Wang, X.Z. (2013). Mutation spectrum of GATA4 associated with congenital atrial septal defects. Arch. Med. Sci. *9*, 976–983. https://doi.org/10.5114/aoms.2013.39788.
39. Yang, Y.Q., Wang, J., Liu, X.Y., Chen, X.Z., Zhang, W., Wang, X.Z., Liu, X., and Fang, W.Y. (2012). Novel GATA4 mutations in patients with congenital ventricular septal defects. Med. Sci. Mon. Int. Med. J. Exp. Clin. Res. *18*, CR344-350. https://doi.org/10.12659/msm.882877.
40. Pietryga, M., Dydowicz, P., Toboła, K., Napierała, M., Miechowicz, I., Gąsiorowska, A., Brązert, M., and Florek, E. (2017). Selected oxidative stress biomarkers in antenatal diagnosis as 11-14 gestational weeks. Free Radic. Biol. Med. *108*, 517–523. https://doi.org/10.1016/j.freeradbiomed.2017.04.020.
41. Toboła-Wróbel, K., Pietryga, M., Dydowicz, P., Napierała, M., Brązert, J., and Florek, E. (2020). Association of oxidative stress on pregnancy. Oxid. Med. Cell. Longev. *2020*, 6398520. https://doi.org/10.1155/2020/6398520.
42. Xie, H.H., Li, J., Li, P.Q., Zhang, A.A., Li, Y., Wang, Y.Z., Xie, D.X., and Xie, X.D. (2017). A genetic variant in a homocysteine metabolic gene that increases the risk of congenital cardiac septal defects in Han Chinese populations. IUBMB Life *69*, 700–705. https://doi.org/10.1002/iub.1651.
43. Malik, R.A., Lone, M.R., Ahmed, A., Koul, K.A., and Malla, R.R. (2017). Maternal hyperhomocysteinemia and congenital heart defects: a prospective case control study in Indian population. Indian Heart J. *69*, 17–19. https://doi.org/10.1016/j.ihj.2016.07.014.
44. Rosenquist, T.H., Ratashak, S.A., and Selhub, J. (1996). Homocysteine induces congenital defects of the heart and neural tube: effect of folic acid. Proc. Natl. Acad. Sci. USA *93*, 15227–15232. https://doi.org/10.1073/pnas.93.26.15227.
45. Hobbs, C.A., Cleves, M.A., Melnyk, S., Zhao, W., and James, S.J. (2005). Congenital heart defects and abnormal maternal biomarkers of methionine and homocysteine metabolism. Am. J. Clin. Nutr. *81*, 147–153.
46. Kalisch-Smith, J.I., Ved, N., and Sparrow, D.B. (2020). Environmental risk factors for congenital heart disease. Cold Spring Harbor Perspect. Biol. *12*, a037234.
47. Pu, W.T., Ishiwata, T., Juraszek, A.L., Ma, Q., and Izumo, S. (2004). GATA4 is a dosage-sensitive regulator of cardiac morphogenesis. Dev. Biol. *275*, 235–244. https://doi.org/10.1016/j.ydbio.2004.08.008.
48. Zhao, L., Xu, J.H., Xu, W.J., Yu, H., Wang, Q., Zheng, H.Z., Jiang, W.F., Jiang, J.F., and Yang, Y.Q. (2014). A novel GATA4 loss-of-function mutation responsible for familial dilated cardiomyopathy. Int. J. Mol. Med. *33*, 654–660. https://doi.org/10.3892/ijmm.2013.1600.
49. Li, J., Liu, W.D., Yang, Z.L., Yuan, F., Xu, L., Li, R.G., and Yang, Y.Q. (2014). Prevalence and spectrum of GATA4 mutations associated with sporadic dilated cardiomyopathy. Gene *548*, 174–181. https://doi.org/10.1016/j.gene.2014.07.022.
50. Yang, Y.Q., Wang, M.Y., Zhang, X.L., Tan, H.W., Shi, H.F., Jiang, W.F., Wang, X.H., Fang, W.Y., and Liu, X. (2011). GATA4 loss-of-function mutations in familial atrial fibrillation. Clin. Chim. Acta *412*, 1825–1830. https://doi.org/10.1016/j.cca.2011.06.017.
51. Jiang, J.Q., Shen, F.F., Fang, W.Y., Liu, X., and Yang, Y.Q. (2011). Novel GATA4 mutations in lone atrial fibrillation. Int. J. Mol. Med. *28*, 1025–1032. https://doi.org/10.3892/ijmm.2011.783.
52. Farag, E., Argalious, M., Narouze, S., DeBoer, G.E., and Tome, J. (2002). The anesthetic management of ventricular septal defect (VSD) repair in a child with mitochondrial cytopathy. Can. J. Anaesth. *49*, 958–962. https://doi.org/10.1007/BF03016883.
53. Zhang, Q., Bai, B., Mei, X., Wan, C., Cao, H., Dan, L., Wang, S., Zhang, M., Wang, Z., Wu, J., et al. (2018). Elevated H3K79 homocysteinylation causes abnormal gene expression during neural development and subsequent neural tube defects. Nat. Commun. *9*, 3436. https://doi.org/10.1038/s41467-018-05451-7.

54. An, Y., Xu, W., Li, H., Lei, H., Zhang, L., Hao, F., Duan, Y., Yan, X., Zhao, Y., Wu, J., et al. (2013). High-fat diet induces dynamic metabolic alterations in multiple biological matrices of rats. J. Proteome Res. *12*, 3755–3768. https://doi.org/10.1021/pr400398b.

55. Daud, A.I., Loo, K., Pauli, M.L., Sanchez-Rodriguez, R., Sandoval, P.M., Taravati, K., Tsai, K., Nosrati, A., Nardo, L., Alvarado, M.D., et al. (2016). Tumor immune profiling predicts response to anti-PD-1 therapy in human melanoma. J. Clin. Invest. *126*, 3447–3452. https://doi.org/10.1172/JCI87324.

56. Guo, X., Wang, L., Li, J., Ding, Z., Xiao, J., Yin, X., He, S., Shi, P., Dong, L., Li, G., et al. (2015). Structural insight into autoinhibition and histone H3-induced activation of DNMT3A. Nature *517*, 640–644. https://doi.org/10.1038/nature13899.

57. Barathi, S., Angayarkanni, N., Pasupathi, A., Natarajan, S.K., Pukraj, R., Dhupper, M., Velpandian, T., Muralidharan, C., and Sivashanmugham, M. (2010). Homocysteinethiolactone and paraoxonase: novel markers of diabetic retinopathy. Diabetes Care *33*, 2031–2037. https://doi.org/10.2337/dc10-0132.

STAR★METHODS

KEY RESOURCES TABLE

REAGENT or RESOURCE	SOURCE	IDENTIFIER
Antibodies		
MARS	Abcam	Cat# ab50793, RRID: AB_881492
NF-κB p65	Cell Signaling Technology	Cat# 8242, RRID: AB_10859369
NF-κB p65 (phospho S536)	Cell Signaling Technology	Cat# 3033, RRID: AB_331284
IKK alpha	Cell Signaling Technology	Cat# 2682, RRID: AB_331626
Phospho-IKKα/β (Ser176/180)	Cell Signaling Technology	Cat# 2697, RRID: AB_2079382
GATA4 Monoclonal Antibody	Thermo Fisher Scientific	Cat# MA5-15532, RRID: AB_10989032
NPPA	Abclonal	Cat# A14755, RRID: AB_2761631
TNNI3	Abclonal	Cat# A0152, RRID: AB_2756984
MYL1	Abclonal	Cat# A8438, RRID: AB_2770495
SOX17	Abclonal	Cat# A18858, RRID: AB_2862485
ETS1	Abcam	Cat# ab225868
Flag	Abmart	Cat# M20008; RRID: AB_2713960
HA	Abmart	Cat# M20003
Actin	Genscript	Cat# A00702-100, RRID: AB_914102
Goat anti-Rabbit IgG (H + L) Highly Cross-Adsorbed Secondary Antibody, Alexa Fluor™ Plus 488	Thermo Fisher Scientific	Cat# A32731, RRID: AB_2633280
Anti-mouse secondary antibody	Genscript	Cat# A00160, RRID: AB_1968937
Anti-rabbit secondary antibody	Genscript	Cat# A00098, RRID: AB_1968815
K-Hcy antibody	This Study	N/A
Biological samples		
Serum Samples from pregnant women as 9–11 weeks of gestation	This Study	N/A
Chemicals, peptides, and recombinant proteins		
Lipofectamine 3000	Invitrogen	Cat# L3000015
Cycloheximide	MedChemExpress	Cat# HY-12320
Palmitic acid	Sigma Aldrich	Cat# P0500
Oleic acid	Sigma Aldrich	Cat# O1008
Stearic acid	Sigma Aldrich	Cat# 85679
Linoleic acid	Sigma Aldrich	Cat# L1376
Eicosatrienoic acid	Yuanye BioTechnology	Cat# Y28446
N-acetyl-L-cysteine	MedChemExpress	Cat# HY-B0215
L-Homocysteine	Sigma Aldrich	Cat# 44925
L-Homocysteine Thiolactone hydrochloride	Sigma Aldrich	Cat# H6503
anti-FLAG M2 affinity gel	Sigma Aldrich	Cat# A2220
anti-FLAG M2 magnetic beads	Sigma Aldrich	Cat# M8823
Folic acid	MedChemExpress	Cat# HY-16637
AHT	N/A	10.15252/emmm.201809469
RNA isolater	Vazyme	Cat# R401-01
Penicillin-Streptomycin	Invitrogen	Cat# 15070063
DAPI	Sigma-Aldrich	Cat# D8417
Critical commercial assays		
Dual-Luciferase Reporter Assay System	Promega	Cat# E1910
Chromatin Immunoprecipitation (ChIP) Assay Kit	Merck	Cat# 17-295
Elecsys Folate III	Roche	Cat# 07027290190

(*Continued on next page*)

Continued

REAGENT or RESOURCE	SOURCE	IDENTIFIER
Homocysteine Enzyme Immunoassay Kit	Axis Shield	Cat# FHCY100
Cell Counting Kit-8	Dojindo	Cat# CK04
FITC Annexin V Apoptosis Detection Kit I	BD Pharmingen	Cat# 556547
DAB Substrate Kit	Beyotime	Cat# P0203
Pierce™ ECL Plus Western Blotting Substrate	Thermo Fisher Scientific	Cat# 32132
HiScript III 1st Strand cDNA Synthesis Kit	Vazyme	Cat# R312-01
ClonExpress MultiS One Step Cloning Kit	Vazyme	Cat# C113-02
ChamQ SYBR Color qPCR Master Mix	Vazyme	Cat# Q411-02
Deposited data		
GC-FID/MS data	MetaboLights	http://www.ebi.ac.uk/metabolights/MTBLS6982
Experimental models: Cell lines		
HL-1	Merck	Cat# SCC065 RRID: CVCL_0303
H9C2	ATCC	Cat# CRL-1446
HEK293T	ATCC	Cat# CRL-11268
Experimental models: Organisms/strains		
C57 BL/6J	Shanghai SLAC Laboratory Animal Co., Ltd.	N/A
Mars heterozygous knockout mice	Gempharmatech	N/A
Sprauge-Dawley rats	Shanghai SLAC Laboratory Animal Co., Ltd.	N/A
Oligonucleotides		
siRNA Oligonucleotides	This Study	Table S5
qRT-PCR primers	This Study	Table S5
ChIP primers	This Study	Table S5
Recombinant DNA		
Mammalian Expression Plasmids	This Study	Table S5
Software and algorithms		
ImageJ	ImageJ	RRID:SCR_003070
Graphpad Prism 8	Graphpad software	https://www.graphpad.com/ RRID:SCR_002798
Proteome Discoverer 2.4	Thermo Fisher Scientific	RRID:SCR_014477
Mascot 2.7.0	Matrix Science	http://www.matrixscience.com RRID:SCR_014322
R 2.17	R studio	https://www.r-project.org/
JASPAR database	JASPAR	http://jaspar.genereg.net RRID:SCR_003030

RESOURCE AVAILABILITY

Lead contact

Further information and requests for resources and reagents should be directed to and will be fulfilled by the lead contact, Jian-Yuan Zhao (zhaojy@vip.163.com).

Materials availability

All reagents generated in this study are available from the lead contact without restriction.

Data and code availability

- GC-FID/MS raw data were deposited in the MetaboLights repository (www.ebi.ac.uk/metabolights/) under the accession number MTBLS6982.
- This paper does not report original code.

- Any additional information required to reanalyze the data reported in this work paper is available from the lead contact upon request.

EXPERIMENTAL MODEL AND SUBJECT DETAILS

Study participants

Human serum samples were obtained from pregnant women who visited the Obstetrics and Gynecology Hospital of Fudan University between January 2018 and December 2019. The study design and conduct were approved and supervised by the Ethics Committee of the Obstetrics and Gynecology Hospital of Fudan University through Ethics Vote 2015-17-C1 in accordance with the criteria established by the Declaration of Helsinki. Written informed consent was obtained from all patients and controls before the start of the study. Serum samples were obtained from women in their first trimester at weeks 9–11 of gestation. The case group included 16 pregnant women bearing children with VSDs and 16 pregnant women bearing children with ASDs. The control group consisted of 32 pregnant women bearing healthy children. CHD phenotypes were first identified by cardiac screening examinations during week 22 of gestation and confirmed after birth using neonatal echocardiography. Participants presenting clinical features of developmental syndromes, multiple major developmental anomalies, known chromosomal abnormalities, or a family history of CHD in a first-degree relative (parent, sibling, or child) were excluded. All participants were unrelated to the ethnic Han Chinese. The demographic characteristics of the pregnant women bearing children with or without CHD are shown in Table S2.

Animal models

C57BL/6 mice were obtained from Shanghai SLAC Laboratory Animal Co., Ltd. (Shanghai, China), housed in polycarbonate cages, and provided food and water at a 12-h light:dark cycle. Male and female mice were paired (1:2 ratio) overnight. Mating was verified by vaginal plug observations the following morning, which was considered E0.5. Pregnant females were randomly assigned to the control and experimental groups ($n \geq 8$ per group).

A high-fatty acid diet-fed pregnant mouse model was established by changing the normal diet to a fatty acid-rich diet from E0.5 to E14.5. The control group was fed with a standard chow diet. The diet composition is shown in Table S4. The rescue groups received N-acetyl-L-cysteine (NAC) at 300 mg/kg or folic acid at 10 mg/kg body weight per day by tail vein injection from E0.5 to E14.5. Embryos were dissected from the decidual capsules in uteri at E14.5 for the analysis of heart defects.

Mars heterozygous knockout mice were generated using the CRISPR-Cas9-mediated genome editing system on a C57BL/6 background by GemPharmatech Co., Ltd. (Jiangsu Province, China). The genotypes of the offspring were identified using PCR. The primers used are shown in Table S5.

All experimental procedures involving animals were approved by the Fudan University Institutional Animal Care and Use Committee and conducted in accordance with the National Institutes of Health Guidelines for the Care and Use of Laboratory Animals.

Cell lines

Rat myoblast cells (H9C2), mouse cardiac cells (HL-1), and human embryonic kidney cells (HEK293T) were cultured in high-glucose Dulbecco's Modified Eagle's Medium (HyClone, South Logan, UT, USA) supplemented with 10% fetal bovine serum (Invitrogen, Carlsbad, CA, USA), 100 units/mL penicillin (Invitrogen), and 100 μg/mL streptomycin (Invitrogen). The cells were incubated in 5% CO2 at 37°C. Cell transfection was performed using Lipofectamine 3000 (Invitrogen) according to manufacturer's instruction. For treatment of fatty acids, 2.5 mM stock solution was prepared, as described previously.55 Each fatty acid was added to the medium for 9 h before harvesting.

Neonatal rat ventricular myocytes culture

Neonatal rat ventricular myocytes (NRVMs) were isolated from 1-day-old Sprauge-Dawley rats. The hearts from 2-day-old rats were aseptically removed and immediately placed in cold PBS buffer. The ventricles were dissected, minced and digested with 0.15% trypsin for 10 min at 37°C and the supernatant was then transferred to a centrifuge tube containing DMEM supplemented with 10% FBS. The steps for digestion were repeated ~10 times to maximize yield. Following centrifugation at 50 x g for 10 min, the cell pellet was resuspended in cultured medium. The suspended cells were plated and incubated at 37°C for 1 h. Thereafter, the culture medium containing non-adherent cells were collected and these enriched cardiomyocytes were seeded in a 24-well plate at a concentration of 1 x 105 cells per well for use in further experiments. 0.1 mM bromodeoxyuridine (BrdU) was added to inhibit fibroblast proliferation.

METHOD DETAILS

Physiological index evaluation of the experimental animals

Pregnant mice were housed individually in cages. Food intake and weight of each pregnant mouse were recorded daily at 9 a.m. from E0.5 to E13.5. Blood pressure, pulse, and random blood glucose of each pregnant mouse were assessed simultaneously every 3 days from E0.5 to E13.5 by using a non-invasive animal blood-pressure meter (Visitech Systems; BP-2000, Apex, New York,

USA) and glucose meter (Accu-chek; Roche, Basel, Switzerland). For glucose tolerance test (GTT), mice were starved for 6 h and injected with glucose (1 g/kg glucose per mouse). Blood glucose level was assessed at 0, 15, 30, 60, and 120 min after injection using a glucose meter.

Mouse embryo heart isolation and histological analysis

Embryonic hearts were dissected at E14.5 and fixed in 4% paraformaldehyde. The hearts were dehydrated using graded ethanol series, followed by vitrification with dimethylbenzene. The heart tissues were embedded in paraffin and sectioned at 5 μm. The sections were then de-paraffinized, rehydrated in graded alcohol series, and stained with hematoxylin–eosin. The stained heart sections were imaged using Olympus IX73 inverted microscope.

Immunohistochemistry

Paraffin embedded heart tissue sections were de-paraffinized twice with xylene and rehydrated. Antigen retrieval was performed in citric acid (pH 6.0) for 10 min. Endogenous peroxidase was blocked with 3% H_2O_2 in methanol. For detection of K-Hcy, sections were incubated with 10mM iodoacetamide resolved in 50 mM Tris-HCl (pH 8.0) for 1 h at room temperature. Samples were then incubated with anti-*p*-IKKα/β (1: 500 dilutions in 10% goat serum) and K-Hcy antibodies (1: 500 dilutions in 10% goat serum) overnight at 4°C, and then the appropriate secondary antibody was applied and incubated at 37°C for 1 h. Sections were developed using a DAB substrate kit (#P0203, Beyotime), and the reaction was stopped with water. The stained heart sections were imaged using Olympus IX73 inverted microscope.

Quantification of metabolites in the plasma

EDTA-treated plasma samples were obtained, centrifuged immediately, and stored in a −80°C freezer until analysis for folate, homocysteine, and triglyceride content. Folate concentration was determined using the Elecsys Folate III competitive chemiluminescent immunoassay (Roche) by using a Cobas E411 Analyzer (Roche). Homocysteine concentration was quantified using the Axis Homocysteine Enzyme Immunoassay Kit (Axis-Shield; Norton, MA). TG, total cholesterol, HDL-C, LDL-C, apolipoprotein A1, apolipoprotein B, FFA, fasting blood glucose, and glycated albumin were analyzed using an automatic biochemical analyzer (Hitachi 7180; WAKO).

Gas chromatography coupled to either a flame ionization detector or mass spectrometer analysis of fatty acids

Gas chromatography coupled to either a flame ionization detector or mass spectrometer (GC-FID/MS) analysis of fatty acids was performed as previously described.[54] In brief, 50 μL of serum samples were added to 600 μL of precooled methanol. Supernatants were collected after 10 min of centrifugation (12,000 × *g*, 4°C). Next, 20 μL of internal standards in hexane (1 mg/mL methyl heptadecanoate, 0.5 mg/mL methyl tricosanoate, and 28 mg/mL butylated hydroxytoluene) were added to a Pyrex tube, followed by the addition of 100 μL of the above supernatant and 1 mL of methanol–hexane mixture (4:1, v/v). The tubes were cooled in liquid nitrogen for 15 min. Next, 100 μL of precooled acetyl chloride was added, and the mixture was flushed briefly with nitrogen gas. The tubes were screw-capped and maintained at 25°C in the dark for 24 h. The tubes were then cooled in an ice bath for 10 min, followed by gradual addition of 2.5 mL of 6% K_2CO_3 solution (with shaking) for neutralization. After the tubes were left to stand for 30 min, 200 μL of hexane was added to extract the methylated fatty acids. The mixture was left to stand for 10 min, and then the upper layer was transferred to a glass sample vial. This extraction process was repeated twice, and the supernatants were combined and evaporated to dryness. The residues were dissolved in 100 μL of hexane and subjected to GC-FID/MS analysis. For tissues, approximately 10 mg of sample was homogenized in 500 μL of methanol by using a TissueLyser at 20 Hz for 90 s. Next, 100 μL of homogenate mixture was transferred to a Pyrex tube for methylation, as described above.

Methylated fatty acids were measured on a Shimadzu GCMS-QP2010Plus spectrometer (Shimadzu Scientific Instruments, USA) equipped with a mass spectrometer with an electron impact (EI) ion source and flame ionization detector (FID). One microliter of the sample was injected into an Agilent DB-225 capillary GC column (10 m, 0.1 mm ID, 0.1 μm film thickness) equipped with a splitter (1:60). Helium gas was used as the carrier and makeup gas. The injection port and detector temperatures were set at 230°C. The column temperature was set at 55°C for 1 min, increased to 205°C at a rate of 30°C/min, maintained at 205°C for 3 min, and increased to 230°C (5°C/min). The MS spectra were acquired using an EI voltage of 70 eV and an *m/z* range of 45–450. Methylated fatty acids were identified by comparing with a chromatogram obtained from a mixture of 37 known standards and confirmed on the basis of mass spectral data. Each fatty acid was quantified using FID data from the signal integrals and internal standards.

Plasmid constructs

Whole-length GATA4 and p65 were amplified from HEK293T or HL-1 cDNA and cloned into the Xho I and EcoR I restriction sites of the pcDNA3.1-Flag vector. Human and mouse *MARS* promoter were amplified from HEK293T or HL-1 genome and cloned into the Xho I and Hind III restriction sites of the pGL3-Basic vector. Plasmids were constructed using ClonExpress MultiS One Step Cloning Kit (#C113-02; Vazyme). The GATA4 mutant was generated by site-directed mutagenesis by using the Mut Express MultiS Fast Mutagenesis kit (#C215-01; Vazyme), according to manufacturer's instructions. The primer sequences were shown in Table S5.

Nuclei and histone isolation

Cells or heart tissues were washed twice with PBS and homogenized in 200 μL of lysis buffer (10 mM HEPES (pH 7.9), 10 mM KCl, 1.5 mM $MgCl_2$, 0.34 M sucrose, 10% glycerol, 1 mM DTT, 0.1% Triton X-100) with protease inhibitor mixture (#4693116001, Sigma-Aldrich). After incubation for 5 min on ice, the nuclei were collected in the pellet by low speed centrifugation (1500 × g, 4 min, 4°C). The nuclei were washed once with the lysis buffer without 0.1% Triton X-100 and then lysed in 200 μL of nuclei lysis buffer (3 mM EDTA, 0.2 mM EGTA, 1 mM DTT, and protease inhibitor mixture). After 10 min incubation on ice, soluble histones were separated from chromatin by centrifugation (2000 × g, 4 min). The supernatants were then added with 10 mM iodoacetamide and reacted for 1h at 4°C before subject to western blotting for detecting homocysteinylated histones.

Immunoprecipitation and western blotting

Cultured cells or cells extracted from the heart tissues were homogenized with 0.5% NP-40 buffer containing 50 mM Tris-HCl (pH 7.5), 150 mM NaCl, 0.5% Nonidet P-40, and a mixture of protease inhibitors. After centrifugation at 12,000 x *g* and 4°C for 15 min, the supernatant of the lysates was collected for western blotting. For immunoprecipitation, cell or tissue lysates were incubated with anti-Flag M2 affinity gel (#A2220, Sigma Aldrich) or specific primary antibodies for 3 h at 4°C. The beads were washed three times with NP-40 buffer before boiling with SDS loading buffer, followed by the standard western blotting procedures. For detection of K-Hcy in cultured cells or heart tissues, 10 mM iodoacetamide was added to the lysates and reacted for 1 h at 4°C before western blotting or immunoprecipitation. Antibodies used are shown in key resources table. Detection was performed by measuring chemiluminescence on a Typhoon FLA 9500 (GE Healthcare, Little Chalfont, UK) using Pierce ECL Plus Western Blotting Substrate (#32132, Thermo Fisher Scientific). The intensity of the blots was qualified using ImageJ.

Preparation of K-Hcy antibody

The pan K-Hcy was generated in our previous study.[24] Briefly, 10 mg chicken egg albumin[55] was homocysteinylated by incubating with 1 mM HTL in 0.1 M Na_2CO_3 (pH 8.0) with 1:10 (v/v) pyridine at 25°C for 14 h. Next, 15 mM iodoacetamide was added and reacted in the dark at room temperature for 1 h. The modified proteins were purified by passing reaction mixtures through a Sephadex G-25 gel filtration column with 50 mM Tris buffer as the mobile phase in an AKTA-FPLC system (GE Healthcare, Chicago, IL, USA) to remove organic reagents. The sample was desalted using a G25 column and dried with a desiccator to obtain a powder as a homocysteine-modified antigen. The antigen was sent to Abmart (Abmart Shanghai Co.,Ltd) to produce K-Hcy antibodies. The specificity of the antibody was validated in our previous study.[24]

RNA extraction and quantitative real-time PCR

Total RNA was isolated from cultured cells or heart tissues by using RNA isolater (Vazyme) and then converted to cDNA by using HiScript III first Strand cDNA Synthesis Kit (#R312, Vazyme). The *Mars, Nppa, Tnni3, Myh7*, *Myl1, Rfc1, Mtr, Dhfr and Mthfr* mRNA levels were measured by quantitative real-time PCR using ChamQ SYBR Color qPCR Master Mix (#Q411, Vazyme) on the ABI Prism 7900 sequence detection system (Applied Biosystems, Foster City, CA, USA), with actin as an internal reference gene. Primers used for qRT-PCR were shown in Table S5.

Dual-luciferase reporter assay

For the *MARS* promoter luciferase reporter assay, HEK293T and HL-1 cells were seeded in a 24-well plate. The cells were transfected with 1 μg of pGL3-*MARS*-promoter plasmid and 20 ng of pRL-TK vector (Promega); half of the cells were additionally co-transfected with 50 ng of the pcDNA3.1-p65 expression plasmid or empty pcDNA3.1 vector by using Lipofectamine 3000. The transfection efficiency was monitored using the Renilla luciferase pRL-TK vector as an internal control. Two days after transfection, cell lysates were collected and subjected to luciferase assay by using the Dual-Luciferase Reporter Assay System (#E1910, Promega), according to manufacturer's protocol. Three independent transfection experiments were performed, and each luciferase assay was performed in triplicate. Normalized data were calculated as the ratio of the Firefly/Renilla luciferase activities.

Electrophoretic mobility shift assay

EMSA was conducted as previously described.[56] Three pairs of 6-carboxy-fluorescein (FAM)-labeled double-stranded DNA probes containing a putative p65-binding site (human, mouse and rat) were generated by annealing their respective complementary oligonucleotides. Probe sequences were shown in Table S5.

HEK293T cells were transfected with pcDNA3.1-p65-Flag or pcDNA3.1-GATA4-Flag plasmids. After 36 h of transfection, cells were harvested and lysed in 0.5% NP-40 buffer, and Flag-tagged proteins were enriched using anti-FLAG M2 magnetic beads (Thermo Fisher Scientific). The FAM-labeled probe (1 pmol) and 20 μg of immunoprecipitated protein were incubated in reaction buffer containing 5 mM $MgCl_2$, 2 mM EDTA, 50 ng/μL poly (dI-dC), 2.5% glycerol, and 0.5 mg/mL BSA for 20 min at 25°C. The reaction mixture without the immunoprecipitated protein was served as a negative control. For the cold competition assay, 50 pmol and 100 pmol unlabelled probes were added into the reaction. The samples were subjected to 10% non-denaturing PAGE and analyzed using a Typhoon FLA 9500 scanner.

Chromatin immunoprecipitation (ChIP) assay

ChIP assay was carried out using the Chromatin Immunoprecipitation (ChIP) Assay Kit (Merck). Briefly, cells were cross-linked by 1% (v/v) formaldehyde for 10 min at 37°C before harvesting. DNA was then sonicated to generate 200- to 500-bp DNA fragments. The sheared chromatin was immunoprecipitated by incubation with p65 or GATA4 antibody or normal rabbit IgG overnight at 4°C. The precipitated DNA fragments were then identified by PCR and quantified by qRT-PCR. Primers are listed in Table S5.

RNAi

Synthetic oligos were used for siRNA-mediated silencing of MARS, RELA, CEBPA, MEIS2, KLF2, MXI1 and TCF4, and scramble siRNA was used as a control. Cells were transfected with siRNAs by using Lipofectamine 3000, according to manufacturer's instructions. Knockdown efficiency was verified using western blotting and qRT-PCR. The siRNA sequences were shown in Table S5.

Sample preparation for LC-MS/MS analysis

For detecting GATA4-interacting proteins and homocysteinylation sites on GATA4, HEK293T cells were transfected with the GATA4-Flag vector and treated with 0.2 mM palmitic acid for 16 h before harvesting. Cells were lysed in 0.5% NP-40 buffer supplemented with 5 mM iodoacetamide (#I1149, Sigma Aldrich) and protease inhibitor (#4693116001, Sigma Aldrich), and the supernatants were then immunoprecipitated with anti-FLAG M2 magnetic beads (M8823-1mL; Sigma Aldrich) for 3 h at 4°C. For detecting K-Hcy sites of GATA4 from heart tissues, heart tissues were homogenized in 0.5% NP-40 buffer supplemented with 5 mM iodoacetamide and protease inhibitor, and the supernatants were then immunoprecipitated with anti-GATA4 antibody. For detecting K-Hcy sites, the precipitates were washed twice with 0.1% NP-40 buffer, twice with ddH_2O, and three times with 50 mM NH_4HCO_3, after which on-bead tryptic digestion was performed at 37°C overnight. The peptides in the supernatants were collected through centrifugation and dried in a speed vacuum (Eppendorf). The obtained peptides were stored at −80°C until LC-MS/MS analysis.

LC-MS/MS analysis

Samples were analyzed on a Q Exactive HF-X mass spectrometer (Thermo Fisher Scientific, Rockford, IL, USA) coupled with high-performance liquid chromatography (EASY-nLC 1200 System; Thermo Fisher Scientific). Dried peptide samples were re-dissolved in Solvent A (0.1% formic acid in water) and loaded onto a trap column (100 μm × 2 cm, home-made; particle size, 3 μm; pore size, 120 Å; SunChrom, USA) with a maximum pressure of 280 bar by using Solvent A, and then separated on an in-house 150 μm × 12 cm silica microcolumn (particle size, 1.9 μm; pore size, 120 Å; SunChrom, USA) with a gradient of 5%–35% mobile phase B (acetonitrile and 0.1% formic acid) at a flow rate of 600 nL/min for 75 min. The MS analysis for Q Exactive HF-X was performed using one full scan (300–1,400 *m/z*, R = 60,000 at 200 *m/z*) at automatic gain control target of $3e^6$ ions, followed by up to 20 data-dependent MS/MS scans with higher-energy collision dissociation (target, 2×10^3 ions; maximum injection time, 40 ms; isolation window, 1.6 *m/z*; normalized collision energy, 27%). Detection was performed using Orbitrap (R = 15,000 at 200 *m/z*). Data were acquired using Xcalibur software (Thermo Fischer Scientific).

K-Hcy site identification

RAW files were processed with UniProt Homo Sapiens (UP000005640) or *Mus musculus* (UP000000589) protein database and using Proteome Discoverer (version 2.4, Thermo Fisher Scientific) with Mascot (version 2.7.0, Matrix Science). The ptmRS node was used in K-Hcy sites analysis workflow. The mass tolerances were 10 ppm for precursor and fragment Mass Tolerance 0.05 Da. Up to two missed cleavages were allowed. The acetylation on the protein N-terminal, oxidation on methionine and carbamidomethylation on cysteine were set as variable modifications. For searching for K-Hcy peptides, carbamidomethylated Hcy on lysine [C(6)H(10)N(2)O(2)S, 174.046 Da] was set as variable modification. False discovery rate (FDR) thresholds for peptide were set to 0.01.

Hcy and HTL quantification

Heart tissues were homogenized on ice-cold PBS (PBS) and centrifuged (10,000 x g) at 4°C for 15 min, and the supernatants were collected for Hcy quantification. Hcy concentration was determined using an Axis Homocysteine Enzyme Immunoassay Kit (Axis-Shield). HTL was assayed as the following: heart tissues were harvested by PBS washing followed by denaturing by pre-chilled 80% methanol (dissolved in ddH_2O, precooled in −80°C). The lysate was centrifuged (10,000 x g) at 4°C for 10 min. The supernatant was vacuum dried, then re-dissolved in ddH_2O and subjected to ultra-filtration on a polyvinylidene fluoride low protein binding membrane (Millex-GV4 and Millex-HV4, Millipore). The collected metabolites were extracted and the HTL was analyzed using liquid chromatography-mass spectrometry (LC-MS) as previously described.[57]

Cell proliferation and apoptosis assay

Cell viability was assessed using the Cell Counting Kit-8 (Dojindo) according to the manufacturer's guidelines. Briefly, a total of approximately 5×10^3 cells were seeded in 96-well plates, 10 μL CCK-8 solution was added to each well and cultivated for 1 h. The absorbance of the reaction system was measured spectrophotometrically at 450 nm. Cell apoptosis was detected using an Annexin V-FITC Apoptosis Detection Kit (BD Pharmingen) according to the manufacturer's guidelines. Data were collected on an Accuri C6 flow cytometer (BD Biosciences).

Immunofluorescence

For detecting subcellular localization of GATA4 and K300W mutants, HL-1 cells were transfected with Flag-tagged GATA4 and K300W mutant for 36 h. Cells were harvested and washed with PBS buffer twice to remove the remaining medium. Paraformaldehyde (4%) was used to fix the cells, 0.5% Triton X-100 in PBS was added and incubated for 20 min at 25°C. Then the cells were incubated with 5% goat serum for 1 h at room temperature and followed by incubating with anti-Flag antibody (1:500 in 5% goat serum) at 4°C overnight. After washing with PBS, cells were incubated with Alexa Flour 488 donkey anti-rabbit secondary antibody for 1 h at 25°C in the dark. Cells were washed and incubated with DAPI for 5 min to display the nuclei. Cells were observed under a fluorescence microscope (Olympus FV3000, Tokyo, Japan).

QUANTIFICATION AND STATISTICAL ANALYSIS

Two-tailed *t*-tests and ANOVA *F*-tests were used to analyze the association of each FFA during human pregnancy with CHD risk in the offspring. The contribution of each FFA to CHD risk was further assessed by taking the permutation variable importance, which measures the contribution of an FFA by randomly shuffling values for that FFA and observing the most important FFAs in the random forest model. Pearson's correlation coefficient was used to measure the association between different FFAs. Pooled results were expressed as the mean or SEM. A one-way ANOVA was performed for multi-group analyses, and two-tailed Student's *t*-tests or *t*-tests with Welch's correction were performed for two-group analyses. Differences were considered statistically significant if the p value was less than 0.05. Statistical analyses were performed using Prism software (version 8.0; GraphPad Software, Inc.), Excel (Microsoft Corp.), and R version 2.17.